Stimulus-Dependent Dopamine Dynamics from Locus Coeruleus Axons

Avi Matarasso[1,2,3] | Itzel Rodriguez Reyes[3,4] | Elena Seaholm[1,3] | Ashritha Cheeyandira[3,4] | Michael J Seibert[2,3] | Suchitha Jagalur[3,5] | Sean C. Piantadosi[2,3] | Li Li[2,3,6] | Yulong Li[7] | David Weinshenker[8] | Michael R. Bruchas[1,2,3,9,*]

[1]Department of Bioengineering, University of Washington, Seattle, WA, USA

[2]Department of Anesthesiology and Pain Medicine, University of Washington, Seattle, WA, USA

[3]Center for the Neurobiology of Addiction, Pain and Emotion; Departments of Anesthesiology, Pharmacology, and Bioengineering, University of Washington, Seattle, WA, USA

[4]Department of Biology, University of Washington, Seattle, WA, USA

[5]Department of Neuroscience, University of Washington, Seattle, WA, USA

[6]Norcliffe Foundation Center for Integrative Brain Research, Seattle, WA, USA

[7]State Key Laboratory of Membrane Biology, Peking University School of Life Sciences, Beijing, China

[8]Department of Human Genetics, Emory University School of Medicine, Atlanta,GA, USA

[9]Department of Pharmacology, Rice University, Houston, TX, USA

Correspondence
Email: mbruchas@uw.edu

Abstract

Arousal is essential for survival, and maladaptive arousal processing leads to an inability to focus, anxiety-like behavior, and dysregulated affective states. Norepinephrine (NE) is known to regulate anxiety, arousal, and learning through locus coeruleus (LC) projections throughout the brain. Evidence for co-release of the NE precursor and neurotransmitter dopamine (DA) from LC neurons has been accumulating for years, yet definitive measures of DA release across regions, stimulus paradigms, and behaviors associated with the LC-NE system remain controversial. Here, we identified the physiological and behavioral properties that evoke DA release from LC axon terminals. Using concomitant approaches, we inhibited the LC and ventral tegmental area (VTA) to selectively isolate the contributions of LC-derived DA release. Together these findings establish the constraints by which LC neurons release DA in a modality-dependent manner.

KEYWORDS

locus coeruleus | dopamine | hippocampus | norepinephrine | optogenetics | fiber photometry | neuromodulation

1 | INTRODUCTION

The locus coeruleus-norepinephrine (LC-NE) system consists of a widespread projecting network of neurons that modulate a range of behaviors like arousal (Berridge 2008, Carter et al. 2010), learning (Bouret and Sara 2004, Kaufman et al. 2020, Seo et al. 2021), and stress-induced negative affect (Giustino et al. 2020, McCall 2015, McCall et al. 2017). As an obligate precursor for NE, dopamine (DA) is also produced in LC neurons. However, because tyrosine hydroxylase (TH; converts tyrosine to L-DOPA), not dopamine β-hydroxylase (DBH; converts DA to NE), is rate-limiting for catecholamine synthesis under normal circumstances (**?**), LC neurons were classically thought to release NE but not DA. Yet, the potential for DA release from noradrenergic neurons has been discussed since the early 2000s. Initially, microdialysis was used to detect neuromodulator release with autoreceptor antagonists (which disinhibit NE or DA neuron activity), and revealed the potential for noradrenergic release of DA. For example, α2 adrenergic receptor (α2ARs) antagonists, but not a D2 dopamine receptor antagonist, upregulated DA release in the occipital cortex (OCC) and medial prefrontal cortex (mPFC), brain regions with very sparse dopaminergic innervation (Borgkvist et al. 2011, Devoto et al. 2003 2004 2005a). Furthermore, LC stimulation increased

Abbreviations: LC, locus coeruleus; DA, dopamine; *Dbh*, dopamine beta hydroxylase; NE, norepinephrine; BLA, basolateral amygdala

the amount of extracellular DA in mPFC and in OCC, which was diminished after local tetrodotoxin administration in mPFC or OCC (Devoto et al. 2005b). Overall, these data suggest that α2ARs on LC axonal terminals regulate release of DA (Devoto et al. 2005a 2003).

While DA could be evoked from noradrenergic neurons through α2AR antagonist administration, whether noradrenergic-sourced DA release affects behavior remained unclear. To investigate the role of LC-DA in behavior, studies employed LC terminal stimulation in the dorsal hippocampus (CA1) and found that spatial awareness and memory were enhanced (Kempadoo et al. 2016, Takeuchi et al. 2016). Infusion of high concentrations of D1 receptor antagonists in CA1 reversed these enhanced spatial memory effects, while blocking β-adrenergic receptors (βARs) had no impact.

These studies implicate LC-evoked DA release in behavior for the first time, but the durations and intensities employed in optogenetics experiments (Gálvez-Márquez et al. 2022, Kempadoo et al. 2016, Takeuchi et al. 2016) do not reflect the LC's established neuronal activity during many of these tasks (Devilbiss and Waterhouse 2011, Kelberman et al. 2024). Pharmacological manipulations in these studies also do not preclude potential circuit level or non-selective effects of these manipulations. Moreover, a ventral tegmental area (VTA) to CA1 dopaminergic circuit controls persistent contextual memory (Lisman and Grace 2005) and contextual fear acquisition in the absence of noradrenergic signaling (Tsetsenis et al. 2021), affirming the need to determine the physiological and behavioral stimuli which evoke DA release from LC axons. There remains limited direct evidence for release of DA from LC terminals *in vivo* in response to appetitive, aversive, or neutral stimuli.

Previous studies detecting LC-evoked DA release utilized microdialysis, which while highly sensitive, lack temporal resolution (Kempadoo et al. 2016, Takeuchi et al. 2016). In contrast, recently developed genetically-encoded biosensors have risen to prominence for neuromodulator detection due to their high temporal resolution and selectivity for target ligands. However, G protein-coupled receptors (GPCRs) have can have non-selective affinity for off-target neuromodulator-GPCRs of similar subclasses and derivatives, and off-target binding has been reported, specifically with NE and DA (López et al. 2024). So while GPCR-based sensors have become widely-used for understanding behavior at relevant time-scales, studies must carefully consider the local innervation of their targeted circuit for off-target neuromodulator release that may inadvertently activate endogenous receptors and sensors (López et al. 2024).

In this study, we consider the controversy surrounding LC-derived DA and how we may measure NE and DA dynamics in regions where there are some overlapping DA and NE inputs. Emerging evidence suggests LC neurons innervate regions with functional specificity and distinct subsets of neurons activate depending on behavioral state (Chandler et al. 2019, Dupret et al. 2010, Nakahara et al. 2004, Poe et al. 2020, Sinha et al. 1999, Uematsu et al. 2017). For example, during early extinction of conditioned fear, LC projections to basolateral amygdala (BLA) are preferentially active. By contrast, during late extinction when mice exhibit diminished fear behavior, LC projections to mPFC are active (Uematsu et al. 2017). The BLA is critical for cued fear (Campeau and Davis 1995, Davis and Whalen 2001, Fanselow and LeDoux 1999, Maren 2001, **?**, Phillips and LeDoux 1992) while CA1 is necessary in contextual fear conditioning (Anagnostaras et al. 1999, Maren et al. 1994, **?**, Phillips and LeDoux 1992), and both are also activated by salient stimuli (Barth et al. 2023, Liu et al. 2021, Schoenbaum et al. 1999, Shukla and Chattarji 2022, Uwano et al. 1995) and reward-associated cues (Ambroggi et al. 2008, Gauthier and Tank 2018, Martig and Mizumori 2011, Paton et al. 2006, Tye and Janak 2007, Uwano et al. 1995, Yun et al. 2023). Therefore, the BLA serves as a critical region alongside the hippocampus to further determine the specific nature of LC-evoked DA dynamics.

Since distinct subsets of LC neurons are activated in response to salient, aversive, and appetitive stimuli (Borodovitsyna et al. 2018, Chandler et al. 2019, Chen and Sara 2007, Curtis et al. 2012, de Medeiros et al. 2005, Grimm et al. 2024, McCall et al. 2017, Poe et al. 2020, Privitera et al. 2024, Silveira et al. 1993) in different behavior states, we hypothesized that DA release from the LC would be greater in BLA than in CA1 during both aversive and appetitive stimuli, as salient stimuli are often associated with BLA activity (Liu et al. 2021, Uwano et al. 1995) and the CA1 receives little dopaminergic input (Tsetsenis et al. 2021). We first established the selectivity constraints and demonstrated high selectivity of the sensors we used. We next demonstrated that we can evoke DA release from LC-CA1 terminals in 2-photon *ex vivo* slice imaging and then found that LC-evoked DA signal follows an increasing linear trend with frequency *in vivo* in CA1 and BLA. We next established the NE and DA responses to appetitive and aversive stimuli in the BLA and CA1. Finally, we used chemogenetics to demonstrate that following appetitive and aversive stimuli, the LC contributes more to endogenous DA release in the BLA than in CA1. Together, we report that LC releases DA with both projection and stimulus specificity. As diminished DBH has been associated with increased vulnerability to psychosis (Cubells et al. 2000, Meltzer et al. 1976, Yamamoto et al. 2003) and neurodegeneration in Parkinson's disease (Lieberman et al. 1972, Nagatsu et al. 1982), characterizing the ratio of DA/NE release by the LC may help determine the neural mechanisms behind these diseases.

2 | RESULTS

$GRAB_{NE}$ does not detect DA *in vivo* in response to biologically relevant photostimulation

Because activation of catecholamine sensors by the off-target catecholamine (DA in the case of $GRAB_{NE2m}$) has been reported (López et al. 2024), it is important to test the limitations of these sensors *in vivo*. If ligand selectivity of each biosensor is not considered, then the results of the stimuli-dependent release could be misconstrued, across any region where dual NE and DA innervation is present. We compiled the most updated EC50s generated in vitro (i.e. the presumed KD due to lack of G-protein coupling) for DA and NE at each GPCR-based sensor for examining the difference in DA vs NE selectivity (Figure 1A) (Feng

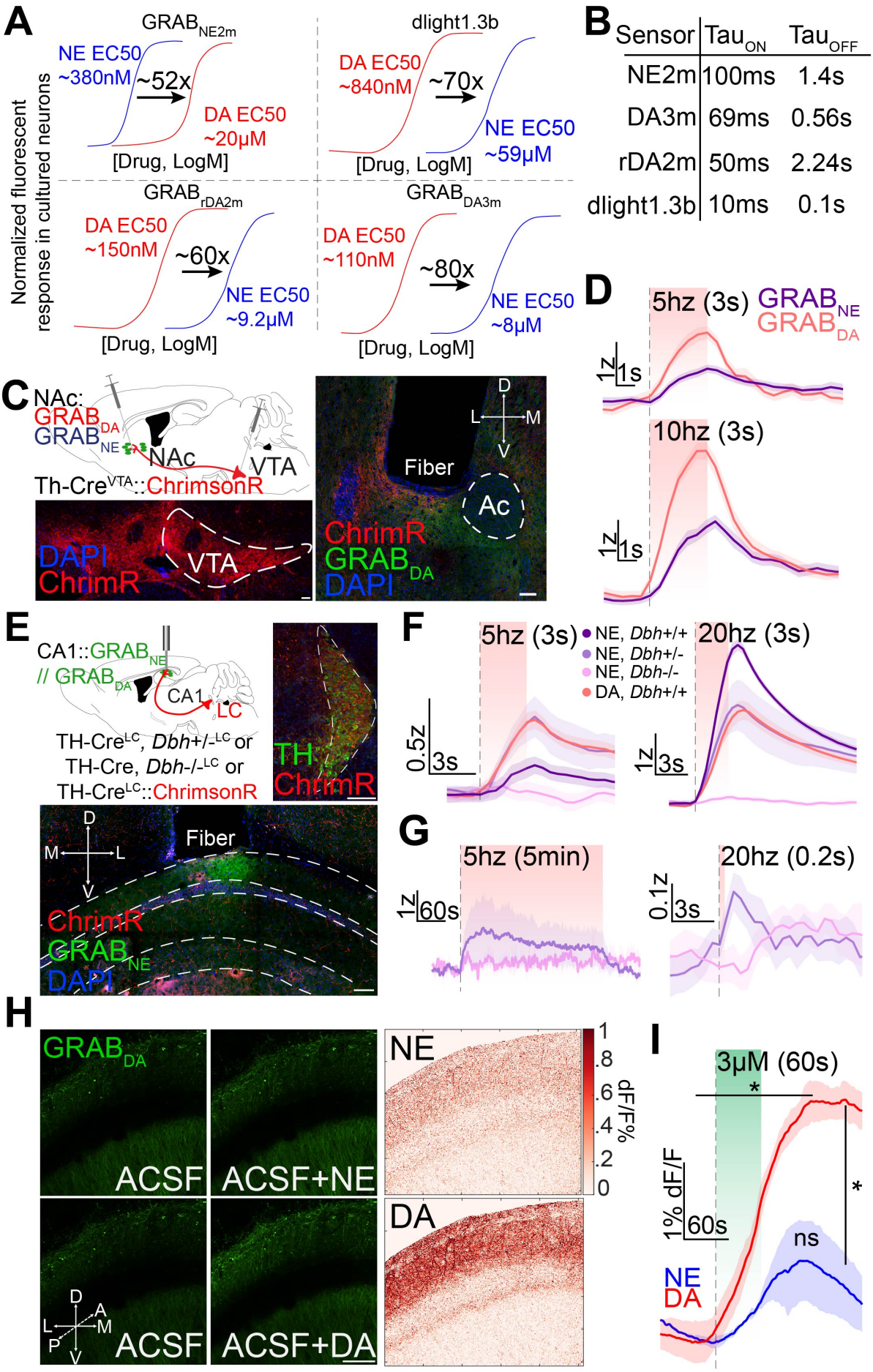
A
GRAB NE2m
NE EC50 ~380nM
~52x
DA EC50 ~20μM
[Drug, LogM]
dlight1.3b
DA EC50 ~840nM
~70x
NE EC50 ~59μM
[Drug, LogM]
GRAB rDA2m
DA EC50 ~150nM
~60x
NE EC50 ~9.2μM
[Drug, LogM]
GRAB DA3m
DA EC50 ~110nM
~80x
NE EC50 ~8μM
[Drug, LogM]
Normalized fluorescent response in cultured neurons
B
Sensor | Tau ON | Tau OFF
NE2m | 100ms | 1.4s
DA3m | 69ms | 0.56s
rDA2m | 50ms | 2.24s
dlight1.3b | 10ms | 0.1s
C
NAc:
GRAB DA
GRAB NE
NAc
VTA
Th-Cre VTA::ChrimsonR
DAPI
ChrimR
VTA
Fiber
Ac
ChrimR
GRAB DA
DAPI
D
5hz (3s)
GRAB NE
GRAB DA
1z
1s
10hz (3s)
1z
1s
E
CA1::GRAB NE
// GRAB DA
CA1
LC
TH-Cre LC, Dbh+/- LC or
TH-Cre, Dbh-/- LC or
TH-Cre LC::ChrimsonR
TH
ChrimR
Fiber
ChrimR
GRAB NE
DAPI
F
5hz (3s)
NE, Dbh+/+
NE, Dbh+/-
NE, Dbh-/-
DA, Dbh+/+
20hz (3s)
0.5z
3s
1z
3s
G
5hz (5min)
1z
60s
20hz (0.2s)
0.1z
3s
H
GRAB DA
ACSF
ACSF+NE
NE
DA
dF/F%
1
.8
.6
.4
.2
0
ACSF
ACSF+DA
I
3μM (60s)
*
1% dF/F
60s
ns
*
NE
DA

FIGURE 1 Biosensors are sufficiently selective for their respective ligand. (a) Concentration response curves of various sensors used in this study for NE and DA. EC50s for both NE and DA and the fold differences are recorded. (b) On and off kinetics of the sensors. (c) Schematic depicts infection of VTA-DA cells with ChrimsonR (AAV5-hSyn-FLEX-ChrimsonR-tdTomato) and $GRAB_{NE}$ or $GRAB_{DA}$ in NAc. Representative image of ChrimsonR expression in VTA cell bodies (bottom) and terminals in NAc (right), with $GRAB_{DA}$ expression in NAc. Scale bar, 100µm. (d) VTA-NAc^{TH} terminal stimulation at 5hz for 3s (top) or 10hz for 3s (bottom) E. Schematic of experimental approach for Th-cre, Dbh-/-, and control Dbh+/- heterozygous mice. ChrimsonR was injected into LC (right) and $GRAB_{NE}$ in CA1 (bottom). Scale bar, 100µm. F. Averaged $GRAB_{NE}$ and $GRAB_{DA}$ responses to LC-CA1 stimulation during different stimulation paradigms (left to right) 5hz (3s) and 20hz (3s). G. Averaged $GRAB_{NE}$ responses to tonic (left) and phasic (right) LC-CA1 stimulation during different stimulation paradigms 5hz 5min (left) and 20hz 200ms (right). Dbh(-/-) indicates Dbh-KO mice, n=3, while Dbh+/- indicate heterozygous controls, n=2, and Dbh+/+ are Th-cre mice, n=9 for $GRAB_{NE2m}$, n=3 for $GRAB_{DA3m}$. H. Representative images of baseline (left) and 3µM NE (middle top) or 3µM DA (middle bottom) washes, with heatmaps (right) showing change in fluorescence (ΔF/F). Scale bar, 100µm. I. Averaged traces of 3µM NE and 3µM DA washes. n=2.

et al. 2024 2019, Patriarchi et al. 2018, Sun et al. 2020). Among the available sensors, the most selective DA sensor is $GRAB_{DA3m}$, with an EC50 of 110nM for DA and 8µM for NE, representing an 80-fold difference in selectivity. The next most selective DA sensor at the time of this study was dLight1.3b, which has a 70-fold difference in selectivity, but also has a larger EC50 for NE than other sensors, at 59µM. $GRAB_{rDA2m}$ has a 60-fold difference in selectivity, and similar EC50s for NE and DA compared to $GRAB_{DA3m}$. Compared to dLight, the $GRAB_{DA3m}$ sensors have a higher affinity for both the target catecholamine and for the non-targeted catecholamine. NE has less affinity at $GRAB_{NE2m}$ than DA has at $GRAB_{DA3m}$ sensors. Comparing on/off kinetics of these catecholamine biosensors is a powerful method of determining separability of recorded signals. The dLight1.3b sensor has a τ_{on} (10ms) 5-7 times faster than $GRAB_{DA3m}$ (69ms) and $GRAB_{rDA2m}$ (50ms) (Figure 1B). While they have a similar τ_{on} rate (50-69ms), the red $GRAB_{rDA2m}$ sensor has τ_{off} (2.24s) 4 times slower than the $GRAB_{DA3m}$ sensor (0.56s). Here, we use these kinetics to compare neuromodulator recordings during behavior and qualitatively explain the likely separability of simultaneously recorded signals.

$GRAB_{NE}$ does not detect DA *in vivo* in response to biologically relevant photostimulation

In this study, we employed several catecholamine sensors to understand DA release from LC. The rank order of selectivity (from highest to lowest) of DA sensors is $GRAB_{DA3m}$ (80x NE/DA, EC50NE = 8µM), dlight1.3b (70x, EC50NE = 59µM), $GRAB_{rDA2m}$ (60x, EC50NE = 9.2µM) (Feng et al. 2024 2019, Patriarchi et al. 2018). $GRAB_{NE2m}$ has a 52-fold difference between NE and DA, with EC50DA= 20µM. Because $GRAB_{NE2m}$ has the lowest fold-difference in selectivity, we tested $GRAB_{NE}$'s selectivity by stimulating VTA terminals in BLA and CA1 *in vivo*. We injected either $GRAB_{NE2m}$ or $GRAB_{DA3m}$ in the BLA or CA1 and Cre-dependent viral vectors containing the red-shifted excitatory opsin ChrimsonR, AAV5-hSyn-DIO-ChrimsonR-tdTmto, into the VTA of Th-cre mice (Th-cre::VTA:ChrimsonR) (Figure S1A).

To evoke DA release from VTA terminals, we mimicked sustained low tonic activation (5hz for 30s) and brief, phasic activation (20hz for 3s) that would not inherently be rewarding (Millard et al. 2024) to determine if DA release binds to $GRAB_{NE2m}$. First, we stimulated VTA terminals in BLA and found $GRAB_{NE2m}$ signal increased during both stimulation paradigms (Figure S1B). We found that when we stimulated VTA terminals in CA1, there were also subtle increases in $GRAB_{NE2m}$ fluorescence (Figure S1C). To assess these results further, we repeated this experiment in a region with substantially less NE innervation by stimulating VTA terminals in the nucleus accumbens (NAc) (Figure 1C), which we expected to produce a heightened $GRAB_{DA3m}$ signal. We detected increased $GRAB_{DA3m}$ fluorescence, but a modest $GRAB_{NE2m}$ signal was still detected in response to VTA-NAc stimulation (Figure 1D). Considering that the NAc contains a 1:10 ratio of NE to DA (Koob et al. 1975), we recognized the need to detect $GRAB_{NE2m}$ signal in a completely NE-deficient environment.

To do so, we stimulated LC-CA1 terminals in mice globally deficient in DBH, rendering them unable to produce NE. We expressed AAV5-hSyn-DIO-ChrimsonR-tdTmto in the LC of Dbh(+/+) mice (Dbh-cre::LC:ChrimsonR), Dbh(+/-) mice (Th-cre, Dbh(+/-)::LC:ChrimsonR) that have similar NE content to Dbh(+/+) mice, or Dbh(-/-) mice (Th-cre, Dbh(-/-)::LC:ChrimsonR), and $GRAB_{NE2m}$ in CA1 (Figure 1E). We found that Dbh(-/-) mice had no increase in $GRAB_{NE2m}$ fluorescence when photostimulating for 3 seconds at 5hz or 20hz (Figure 1F). In contrast, $GRAB_{NE2m}$ fluorescence increased in response to LC-CA1 photostimulation in both Dbh(+/+) and heterozygous Dbh(+/-) mice (Figure 1F). Similarly, in response to LC-CA1 photostimulation at both 5hz and 20hz, we detected robust increases in $GRAB_{DA3m}$ signal in Dbh(+/+) mice (Figure 1F-G). These data suggest that in response to LC-CA1 stimulation in the absence of NE production, $GRAB_{NE2m}$ does not detect NE and $GRAB_{DA3m}$ is detecting DA.

The qualitative differences in $GRAB_{NE2m}$ signal between Dbh(+/+) and Dbh(-/-) mice is likely due to differences in strain background (C57Bl/6J and mixed C57Bl/6J;129SvEv, respectively). To simulate physiological LC activity at high tonic or phasic activation mimicking exposure to a novel-stimulus, we optogenetically stimulated LC terminals in CA1 at 5hz for 5min or at 20hz for 200ms while recording $GRAB_{NE2m}$ signal. We observed that in both activation paradigms, stimulating LC terminals in heterozygous Dbh(+/-) controls increased $GRAB_{NE2m}$ fluorescence, while the same experiment in Dbh(-/-) mice revealed no activation of $GRAB_{NE2m}$ (Figure 1H). These results indicate that the least selective catecholamine biosensor, $GRAB_{NE2m}$ (Figure 1A), does not detect appreciable increases in $GRAB_{DA3m}$ fluorescence at the

upper boundary of stimulation parameters where we detect DA release from LC axon terminals (Figure 1F).

To further characterize the selectivity of sensors, we used *ex vivo* slice 2-photon imaging to record sensor activity while washing on high concentrations of ligands. We injected either $GRAB_{NE2m}$ or $GRAB_{DA3m}$ in the CA1 of WT mice. After waiting a minimum 5 weeks for expression, we recorded $GRAB_{NE2m}$ or $GRAB_{DA3m}$ fluorescence in coronal hippocampal slices in response to washes using 2-photon imaging (Figure 1H). When we washed 3µM of NE or DA on slices expressing $GRAB_{DA3m}$, respectively, we observed robust increases in $GRAB_{DA3m}$ fluorescence to DA (Sidak's multiple comparisons test, p=0.0115) compared to baseline, no significant change in fluorescence from baseline when NE was washed on (p=0.23), and a significant difference between NE and DA (Sidak's multiple comparisons test, 0.0325). These data suggest $GRAB_{DA3m}$ is responding to DA and not NE in tissue slices at as high a concentration as 3µM.

Ex vivo photostimulation of LC terminals causes release of DA in a frequency-dependent manner

Having demonstrated $GRAB_{NE2m}$ and $GRAB_{DA3m}$'s selectivity over the potential cross-reactive catecholamine, we next sought to better describe the DA release evoked from the LC. To characterize LC-evoked DA release, we used *ex vivo* slice imaging which severs upstream circuit interactions while maintaining local, intact DA release from LC-$CA1^{Dbh}$ terminals. Imaging *ex vivo* also cuts off potential antidromic activation of LC cell bodies and subsequent VTA-DA neuron activation downstream. We injected either $GRAB_{NE2m}$ or $GRAB_{DA3m}$ in the CA1 and Cre-dependent viral vectors containing ChrimsonR, AAV5-hSyn-DIO-ChrimsonR-tdTmto, into the LC of Dbh-cre mice (Dbh-cre::LC:ChrimsonR). After waiting a minimum 5 weeks for expression, we recorded $GRAB_{NE2m}$ or $GRAB_{DA3m}$ fluorescence in coronal hippocampal slices in response to photostimulation of Dbh-cre::LC:ChrimsonR projections (615nm, 5 or 20hz, 5ms pulse width) using 2-photon imaging (Figure 2A). First, we established sensor expression with a positive control wash of 30µM NE or DA on slices expressing $GRAB_{NE2m}$ or $GRAB_{DA3m}$, respectively (Figure 2B). After establishing consistent sensor responses to either NE or DA, we photostimulated LC-$CA1^{Dbh}$ terminals over the full-field, pulsing a 615nm red LED at 5 or 20hz (3 or 30s duration, 5ms pulse width, 3mW) to determine evoked DA release across a range of LC activation intensities. In Figure 2C, an averaged $GRAB_{DA3m}$ trace during 20hz stimulation of LC-$CA1^{Dbh}$ terminals for 30s is provided, indicating robust $GRAB_{DA3m}$ responses to LC-$CA1^{Dbh}$ terminal stimulation.

In both $GRAB_{DA3m}$ and $GRAB_{NE2m}$ expressing CA1 slices, we observed a significant increase in fluorescence across all stimulation paradigms tested (Figure 2D-E). We compared the change in ΔF/F% at each of the stimulation paradigms and found that none of the ΔF/F% changes between $GRAB_{NE2m}$ and $GRAB_{DA3m}$ response were significantly different (Figure 2F). To test the consistency of these results, we repeated these *ex vivo* experiments with dLight expressed in CA1, and ChrimsonR expressed in the LC of Dbh-cre mice (Figure S2A-B, I). We only observed significant increases in fluorescence when we stimulated for 3s at 20hz, while other paradigms were more variable in their detected DA release (Figure S2C). These results indicate DA is released from LC-$CA1^{Dbh}$ terminals *ex vivo*, regardless of any connections from LC to other dopaminergic nuclei.

Evoked LC-NE axonal release *in vivo* follows a frequency-dependent, non-linear relationship

Our *ex vivo* results demonstrate that photostimulating LC-$CA1^{Dbh}$ axon terminals evokes DA release. We next determined how LC-evoked DA release varies across a range of photostimulation paradigms that parallel natural neuronal LC activity *in vivo* (Bourdélat-Parks et al. 2005, Devilbiss and Waterhouse 2011, Szot et al. 1999, Thomas et al. 1998 1995) and examined two target regions. We injected either $GRAB_{NE2m}$ or $GRAB_{DA3m}$ in CA1 or BLA, and Cre-dependent viral vectors containing ChrimsonR, into the LC of Dbh-cre mice (Dbh-cre::LC:ChrimsonR; Figure 2G). We implanted optical fibers above injection sites in BLA and CA1 to record photometric signals during optogenetic stimulation of LC axon terminals.

During periods of low arousal, such as sleep, LC fires tonically at 1-3hz. In high arousal states, like stress, elevated tonic LC-NE neuron firing rates are observed (between 5-10hz) (Aston-Jones and Cohen 2005, Curtis et al. 2012, Devilbiss and Waterhouse 2011, Poe et al. 2020). Recent studies report release of DA from LC-CA1 projections in response to photostimulation at 20hz (Kempadoo et al. 2016, Takeuchi et al. 2016). Thus, we stimulated the LC-$CA1^{Dbh}$ and LC-BLA^{Dbh} projections for 3s at 1, 3, 5, 10, 15, and 20hz with a 5ms pulse width and a total of 10 stimulation trains each session with an interstimulation interval of 1min (Figure 2H-L). We depict a representative averaged response of $GRAB_{NE2m}$ and $GRAB_{DA3m}$ to the stimulation at 15hz for 3s in Figure 2H. We also depict the responses to LC-CA1 stimulation averaged across frequency in Figure 2I for $GRAB_{NE2m}$ recordings and Figure 2J for $GRAB_{DA3m}$ recordings. To characterize trends within each sensor and across regions, we plotted the peak responses across the frequencies tested in CA1 (Figure 2K) and in BLA (Figure 2L). LC-BLA^{NE} and LC-$CA1^{NE}$ release across frequencies strongly matched a second-order polynomial fit (adjusted R^2 values in CA1 was 0.92, BLA was 0.92). LC-$CA1^{DA}$ and LC-BLA^{DA} release across frequencies more closely followed a linear regression model, with adjusted R^2 values of 0.92 in CA1 and 0.96 in BLA (Figure 2L). Further, optically evoked LC-$CA1^{DA}$ release *in vivo* was not significantly different from evoked LC-BLA^{DA} release (Kolmogorov-Smirnov test, n.s., p=0.93; Figure 2K-L). These data suggest that the distributions of LC evoked DA release in different regions are not significantly different.

We repeated these experiments in mice expressing dLight in CA1 and BLA, with Cre-dependent ChrimsonR expressed in the LC of Dbh-cre mice (Figure S2D, I). We repeated *in vivo* stimulation for 3s across the same range of frequencies reported in Figure 2H-L (1-20hz) and depicted averaged responses in Figure S2E, G. We characterized trends in DA dynamics response across frequency and found that, a second-order polynomial was not appropriately fit in the BLA (adjusted R^2 values in BLA was 0.30), although in CA1, a second-order fit was moderately well-fit (R^2 values in CA1 was 0.84; Figure S2F, S2H). These data suggest that

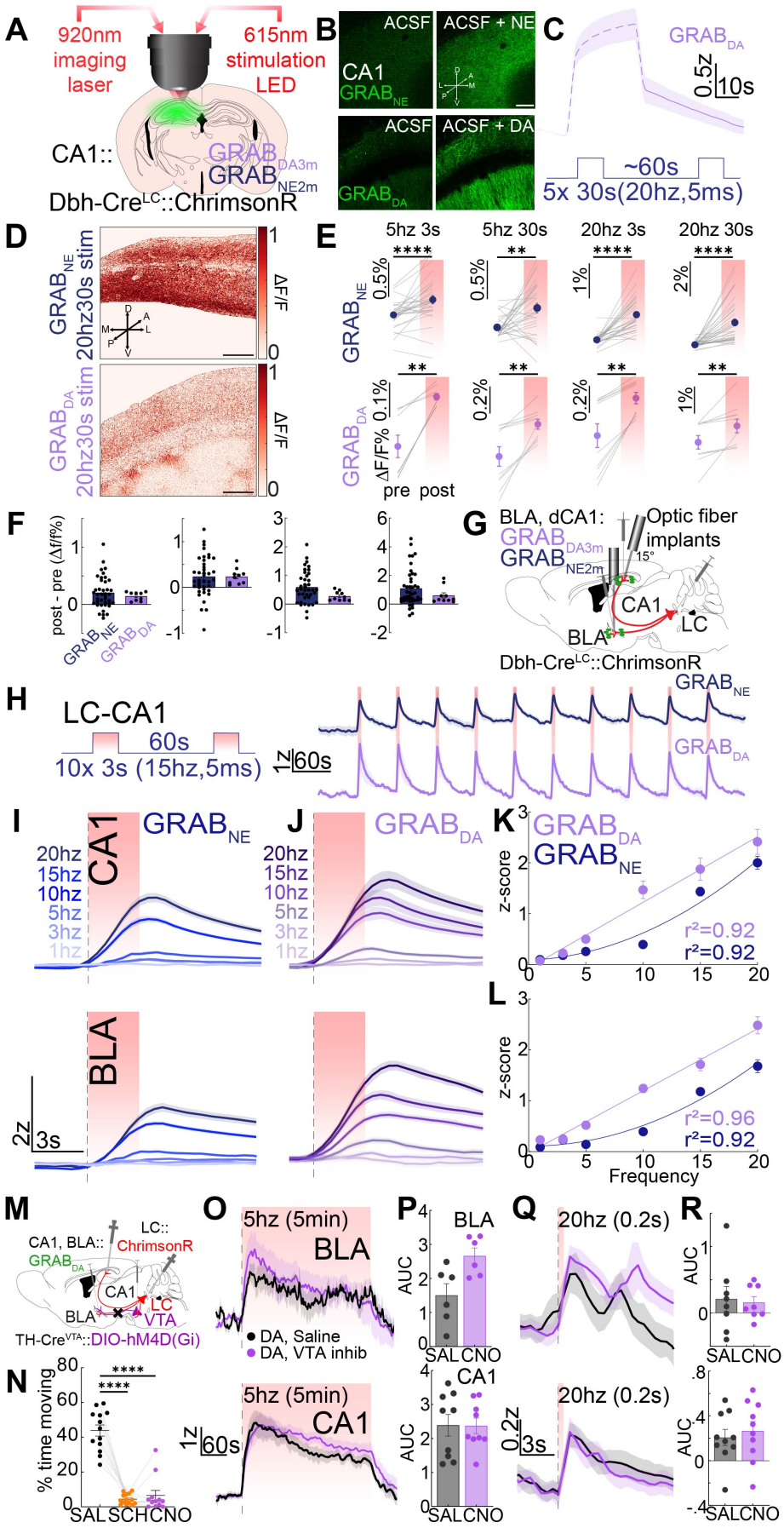
A
920nm imaging laser
615nm stimulation LED
CA1::
GRAB DA3m
GRAB NE2m
Dbh-Cre LC::ChrimsonR
B
ACSF
ACSF + NE
CA1
GRAB NE
ACSF
ACSF + DA
GRAB DA
C
GRAB DA
0.5z
10s
~60s
5x 30s(20hz,5ms)
D
GRAB NE 20hz30s stim
GRAB DA 20hz30s stim
ΔF/F
E
5hz 3s
5hz 30s
20hz 3s
20hz 30s
GRAB NE
GRAB DA
ΔF/F%
pre post
F
post - pre (Δf/f%)
GRAB NE
GRAB DA
G
BLA, dCA1:
GRAB DA3m
GRAB NE2m
Optic fiber implants
15°
CA1
LC
BLA
Dbh-Cre LC::ChrimsonR
H
LC-CA1
60s
10x 3s (15hz,5ms)
1z
60s
GRAB NE
GRAB DA
I
CA1
GRAB NE
20hz
15hz
10hz
5hz
3hz
1hz
BLA
2z
3s
J
GRAB DA
K
GRAB DA
GRAB NE
z-score
r²=0.92
r²=0.92
L
z-score
r²=0.96
r²=0.92
Frequency
M
CA1, BLA::
GRAB DA
LC::
ChrimsonR
CA1
BLA
LC
VTA
TH-Cre VTA::DIO-hM4D(Gi)
N
% time moving
SAL SCH CNO
O
5hz (5min)
BLA
DA, Saline
DA, VTA inhib
5hz (5min)
CA1
1z
60s
P
BLA
AUC
SAL CNO
CA1
Q
20hz (0.2s)
0.2z
3s
R
AUC
SAL CNO

FIGURE 2 Evoked LC-DA axonal release *in vivo* follows a frequency-dependent linear relationship and is independent of VTA activity. (a) Schematic of experimental approach of surgical injections and 2-photon imaging approach with optical stimulation. Schematic depicts infection of LC-NE cells with ChrimsonR (AAV5-hSyn-FLEX-ChrimsonR-tdTomato) and either $GRAB_{DA3m}$ or $GRAB_{NE2m}$ in CA1. (b) Representative 2-p images. 30µM NE was washed on $GRAB_{NE}$ (top), and 30µM DA on $GRAB_{DA}$ (bottom), expressing slices. Rolling average of 5s, scale bar 100µm. (c) Representative average of $GRAB_{DA}$ response to 20hz 30s pulses of optical stimulation of LC-CA1 terminals. Stimulation paradigm depicted below example trace. (d) Heatmap of the $GRAB_{NE}$ (top) and $GRAB_{DA}$ (bottom). ΔF/F response to 20hz 30s stim of LC-CA1 terminals. Δ represents change from right before stimulation, gaussian filter applied to smooth baseline images. (e) ΔF/F% change of pre to post in $GRAB_{NE}$ (top, n=4 biological replicates, 6 slices) and $GRAB_{DA}$ (bottom, n=2) in response to a range of stimulation paradigms: 5hz 3s, 5hz 30s, 20hz 3s, 20hz 30s (left to right). Wilcoxon matched-pairs signed rank test: $GRAB_{NE}$: 5hz 3s, p<0.0001; 5hz 30s, p=0.0019; 20hz 3s, p<0.0001; 20hz 30s, p<0.0001; $GRAB_{DA}$: 5hz 3s, p=0.0039; 5hz 30s, p=0.002; 20hz 3s, p=0.002; 20hz 30s, p=0.002. (f) Schematic of surgical approach for *in vivo* photometry cohort. $GRAB_{DA}$ or $GRAB_{NE}$ were expressed in CA1 and BLA with fiber photometry implants, and ChrimsonR expressed in LC. Scale bar, 100µm. (g) Comparison of the change in ΔF/F response for $GRAB_{NE}$ and $GRAB_{DA}$ in each stim trial from before to after stimulation across the same paradigms in 2E. Mann-Whitney: 5hz 3s, n.s., p=0.96; 5hz 30s, n.s., p=0.91; 20hz 3s, n.s., p=0.09; 20hz 30s, n.s., p=0.27. (h) Average photometry trace of LC-CA1 stimulation for 3s at 10hz, with a 5ms pulse width. n=5. (i) Averaged *in vivo* photometry traces of $GRAB_{NE}$ responses to LC-CA1 (top) and LC-BLA (bottom) terminal stimulation. (j) Averaged photometry traces of $GRAB_{DA}$ responses to LC-CA1 (top) and LC-BLA (bottom) terminal stimulation. (k) Frequency response curves for LC-CA1 terminal stimulation for $GRAB_{NE}$ and $GRAB_{DA}$. Second-order curve fit to $GRAB_{NE}$, n=5-9, r^2= 0.92, and linear regression fit to $GRAB_{DA}$, n=3, r^2= 0.92. (l) Frequency response curves for LC-BLA terminal stimulation for $GRAB_{NE}$, n=6, and $GRAB_{DA}$, n=3. Second-order curve fit to $GRAB_{NE}$, r^2= 0.92, and linear regression fit to $GRAB_{DA}$, r^2= 0.96. (m) Schematic of experimental approach of surgical injections of LC-NE cells with ChrimsonR (AAV5-hSyn-FLEX-ChrimsonR-tdTomato), VTA-DA cells with Gi-DREADDs (AAV5-hSyn1-DIO-HA-hM4D(Gi)), and $GRAB_{DA3m}$ in CA1, of Th-cre mice. (n) VTA inhibition decreased the time mice spent moving. SAL, n=7; SCH, n=7; CNO, n=6. (o) Average trace of $GRAB_{DA}$ response to tonic stimulation (5hz, 5min) of LC terminals in BLA (top; n=8) and CA1 (bottom, n=10), with VTA inhibition (purple) or saline controls (black). (p) AUC for 120s after start of 5hz stimulation for mice injected with saline or CNO (VTA Inhibition). (q) Average trace of $GRAB_{DA}$ response to phasic stimulation (20hz 200ms) of LC terminals in BLA (top; n=8), and CA1 (bottom, n=10). (r) AUC for 3s after start of 20hz, 200ms stimulation for mice injected with saline or CNO (VTA Inhibition).

while NE release from LC follows a second-order relationship, LC evoked DA release follows a linear relationship. This points to likely differences in uptake, autoreceptor activity, metabolism, repletion, or sensor kinetics; the findings nevertheless indicate a potential separation of relevant LC firing properties and the relative NE and DA concentration in each. Further studies using the newest high-resolution FLIM based sensors are needed to mechanistically quantify these findings (Lee et al. 2019, Salinas et al. 2023, Zheng et al. 2025).

DA release from LC axons persists during VTA inhibition

In the 2-photon slice experiments (Figure 2D-H), we severed connections from LC to CA1, preventing antidromic activation of the LC, but local DA neuron axon terminals may still be activated by interactions with evoked NE release via 2AR or 1AR expression on VTA neurons (Bernacka et al. 2022, Boyajian and Loughlin 1987, Greene et al. 2005, Nicholas et al. 1993ba, Rosin et al. 1993). To remove VTA as a source of DA when LC terminals are stimulated, we inhibited the VTA while recording $GRAB_{DA}$ signal. We expressed the Cre-dependent inhibitory designer receptor exclusively activated by designer drugs (DREADD), virally delivered with AAV5-hSyn-DIO-HA-hM4D(Gi) bilaterally in the VTA of Th-cre mice (Th-cre::VTA^{bilat}:Gi-DREADDs), AAV5-hSyn-DIO-ChrimsonR-tdTmto in the LC (Th-cre::LC:Chrimson), and AAV2/9-hSyn-WPRE-PA-$GRAB_{DA3m}$ in CA1 or BLA (Th-cre::CA1 or BLA: $GRAB_{DA3m}$; Figure 2M). When we injected the DREADD agonist clozapine-N-oxide (CNO) (0.5 mg/kg, i.p.) 30min prior to exposing mice to a large open field chamber (50x50cm), we observed a significant decrease in the time the mice spent moving, which were mimicked by the effects of the D1-antagonist SCH23390 (0.25 mg/kg, i.p.) (Figure 2N). D1 dopamine receptors are involved in movement initiation and execution (Hauber 1996, Heath et al. 2015), thus these data indicate that the hM4Di expressed is reliably suppressing DA transmission.

We next tested whether VTA-DA neurons were required for LC-evoked DA release and determined if VTA-DA neuronal involvement in LC-evoked DA release depends on the mode of LC activity. To induce a range of LC activity, we simulated low tonic, high tonic, and phasic stimulation. For low tonic or high tonic stimulation, we stimulated terminals for 5min at either 1hz or 5hz. Photostimulation of LC-$CA1^{Th}$ and LC-BLA^{Th} terminals evoked DA release in response to 5hz (Figure 2O-P). To simulate phasic stimulation, we stimulated LC terminals in BLA and CA1 for 200ms at 20hz, which evoked DA release in both (Figure 2Q-R). When we inhibited the VTA using CNO, evoked DA did not decrease in either 5hz tonic stimulation (Figure 2O-P) or in 20hz phasic stimulation (Figure 2Q-R), indicating the VTA is not necessary for evoking DA release from LC axons. Taken all together, these results further establish that the LC releases DA independent of VTA activity.

Appetitive and aversive stimuli evoke more DA release in BLA compared to CA1

Previously, LC-evoked DA has been suggested to affect behavior, but there are no data that report endogenous DA release during behavior (Kempadoo et al. 2016, Takeuchi et al. 2016). To ascertain whether the LC releases DA endogenously in response to salient stimuli, we first

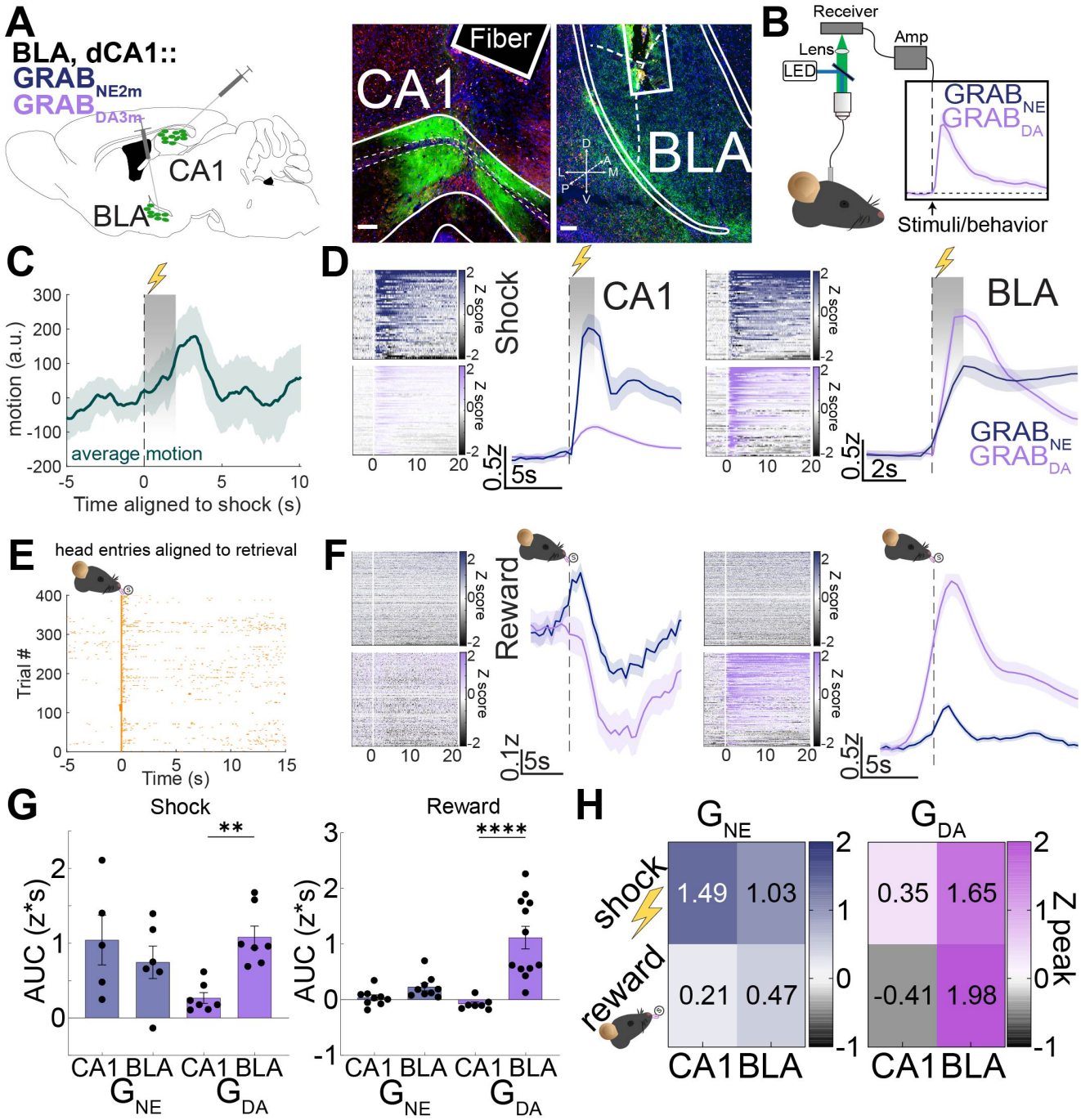

FIGURE 3 Reward and aversive stimuli evoke primarily NE in CA1 and DA in BLA. (a) Schematic of experimental approach depicts infection of cells with $GRAB_{DA}$ (AAV2/9-hSyn-WPRE-PA-DA3m) or $GRAB_{NE}$ (AAV1-hsyn-$GRAB_{NE2m}$) in CA1 and BLA with fiber photometry implants. Scale bar, 100µm. (b) Schematic of photometry acquisition. (c) Average motion aligned to shock in mice experessing $GRAB_{DA}$. (d) $GRAB_{NE}$ and $GRAB_{DA}$ traces in response to 2s shock (0.5mA to 0.7mA) presented with a pseudorandom ITI of 20-90s in CA1 (left, nNE=5, nDA=7) and BLA (right, n_{NE}=6, n_{DA}=7). Heatmaps for $GRAB_{NE}$ and $GRAB_{DA}$ responses to shock with color axes from -2 to 2. (e) Example rasterplot of reward delivery and subsequent head entries in trained mouse. (f) $GRAB_{NE}$ and $GRAB_{DA}$ response to reward in CA1 (left, n_{NE}=9, n_{DA}=7) and BLA (right, n_{NE}=9, n_{DA}=12). Heatmaps for $GRAB_{NE}$ and $GRAB_{DA}$ responses to reward retrieval with color axes from -2 to 2. Sucrose pellets were delivered to hungry mice with a pseudorandom ITI of 30, 60, 90, 120s with an average of 90s. (g) Quantification of the AUC of the average $GRAB_{NE}$ or $GRAB_{DA}$ response to shock (left) or reward (right). Post hoc P-values derived from Kruskal-Wallis with Dunn's multiple comparison. Shock, $GRAB_{DA}$-CA1 vs -BLA, p=0.0095. Reward, $GRAB_{DA}$-CA1 vs $GRAB_{DA}$-BLA, p<0.0001. (h) Heatmap of peak z-scores during both experiments in 3D and 3F. All data are mean ± SEM.; n represents biologically independent mice.

investigated endogenous release of DA and NE in BLA and CA1 in response to simple aversive and appetitive stimuli. To detect NE or DA dynamics, we injected virally-delivered green NE or DA sensors, AAV1-hSyn-$GRAB_{NE2m}$ or AAV2/9-hSyn-WPRE-PA-$GRAB_{DA3m}$, respectively, into the BLA or CA1 (Dbh-cre::CA1 or BLA:$GRAB_{NE2m}$ or $GRAB_{DA3m}$; Figure 3A) of Dbh-cre mice we used in photostimulation experiments in Figure 2. We implanted optical fibers above injection sites in BLA and CA1 to record photometric signal during stimulus administration, including footshock, reward (Figure 3B).

First, mice were exposed to a 2s footshock, a highly salient and aversive stimulus. During the 2s shock, mice moved more than before each shock (Figure 3C). In CA1, $GRAB_{NE2m}$ and $GRAB_{DA3m}$ fluorescence increased at the onset of the shock, with the $GRAB_{DA3m}$ response lower than $GRAB_{NE2m}$ (Figure 3D, left, and Figure S3A-B). In BLA, the $GRAB_{DA3m}$ response was greater than $GRAB_{NE2m}$ in response to shock, but $GRAB_{NE2m}$ had a slow decay for over 30s, which was notably different to the decay in $GRAB_{NE2m}$ signal in response to other stimuli (Figure 3D, right, and Figure S3C-D). Only $GRAB_{NE2m}$ had a sustained and significantly increased signal for the rest of the session compared to baseline (Figure S3I). In response to shock, the BLA-DA response was higher than the CA1-DA response (Figure 3G, Kruskal-Wallis with Dunn's multiple comparison, p=0.0095). These data indicate NE and DA are released in both CA1 and BLA in response to aversive stimuli.

Next, we investigated baseline NE and DA dynamics in response to an appetitive stimulus, the retrieval and consumption of a sucrose reward. We recorded NE and DA dynamics as mice completed the task, and aligned photometry signals to the moment mice entered their heads in the hopper to retrieve sucrose pellets throughout the session (Figure 3E). We found that as mice approached the hopper for reward, NE was released in CA1, and as mice consumed, there was a subtle dip in the $GRAB_{NE2m}$ signal (Figure 3F, left). In the BLA, both NE and DA increased as mice approached the hopper to retrieve a sucrose pellet (Figure 3F, right). In response to shock and reward, $GRAB_{DA3m}$ signal increased in BLA greater than in CA1 (Figure 3G, shock: p=0.0095, reward: p<0.0001), whereas $GRAB_{NE2m}$ signal was not significantly different within each behavior across regions. These data suggest more DA is released in BLA than in CA1 in response to salient stimuli (Figure 3G-H).

In addition to shock and reward delivery, we tested additional types of appetitive and aversive behaviors. First, we used a looming stimulus to simulate a less salient, aversive stimuli, and found that NE was released in CA1 and BLA to the onset of the looming stimulus (Figure S3E). Similar to the footshock, $GRAB_{DA3m}$ signal increased in BLA, but not in CA1, at the onset and offset of the looming stimulus (Figure S3E). Mice also exhibited darting behavior at the onset of the looming stimuli (Figure S3F). To assess a second appetitive behavior, mice were trained to poke their nose in a port for a reward predicted by a 2s light cue, while a second, inactive nose port, led to no reward delivery. When trained mice poked their nose in the correct port, dLight signal in BLA increased in anticipation of the cue-signaling reward (Figure S3G). While the dLight and $GRAB_{NE}$ signal in BLA did not increase to cue, the dLight and $GRAB_{NE}$ signals in BLA increased to reward retrieval and consumption (Figure S3G, top). There was no increase in dLight signal in CA1 during operant paradigm, but there was a decrease in $GRAB_{NE}$ signal to nosepoking for reward (Figure S3G, bottom). When mice poked their noses in the inactive nose port, there was a clear increase in dLight in BLA and a smaller increase in CA1, while there was no increase in $GRAB_{NE}$ signal in BLA or CA1 (Figure S3H). All together, these results establish that we can detect DA that is released in the BLA following both aversive and appetitive stimuli, and DA is only detected in CA1 during salient aversive stimuli.

LC inhibition decreases BLA DA release to appetitive and aversive stimuli

Finally, we sought to conclusively demonstrate that DA released following appetitive and aversive stimulus presentation is from LC-BLA axon terminals. To accomplish this, we used inhibitory chemogenetics to suppress either LC-NE or VTA-DA activity. To accomplish this, we injected the Cre-dependent Gi-DREADD (AAV5-hSyn1-DIO-HA-hM4D(Gi)) bilaterally in the LC of Th-cre mice (Th-cre::LC^{bilat}:Gi-DREADDs) (Figure 4A) and AAV9-hSyn-$GRAB_{rDA2m}$ in the CA1 (Figure 4B) or BLA (Figure 4C).

Because pupil dilation is positively correlated with higher LC activity(Liu et al., 2017; Murphy et al., 2014), we used pupillometry to establish the efficacy of Gi-DREADD inhibition of LC activity (Privitera et al. 2020) (Figure 4D). When we injected the DREADD agonist CNO (0.5 mg/kg, i.p.) in Th-cre mice expressing hM4D(Gi) in LC bilaterally, we observed a consistent, significant decrease in pupil radii compared to saline, as measured by comparing the "area under the curve" (ΔAUC, z*s), suggesting that the LC was inhibited by this chemogenetic approach (Figure 4E-F, paired t-test, p=0.0223).

With DREADD suppression of the LC-NE system established, we next injected either CNO (0.5 mg/kg, i.p.) or saline 30 min prior to a session in which mice received pseudorandom (ITI of 90-150s) delivery of sucrose pellets while recording $GRAB_{rDA2m}$ (Figure 4I) to measure BLA DA release during reward consumption. Following saline administration, as mice retrieved a reward and throughout consumption, DA was released in the BLA before returning to baseline (Figure 4H). Relative to saline treatment, we observed a significant decrease in BLA DA release when mice retrieved and consumed a reward following CNO inhibition of LC (Figure 4H, 1s bins analyzed with 2-way ANOVA, Sidak test for multiple comparisons, p<0.05 for all bins). Comparing the total change in DA release (ΔAUC, z*s), we found LC inhibition significantly reduced DA release in BLA during reward consumption relative to saline (Figure 4I, 2-way ANOVA, with Sidak test for multiple comparisons, p=0.0327). In CA1, we did not observe DA release during reward consumption (Figure 4J-K). In summary, these data indicate that inhibiting the LC during reward retrieval leads to a decrease in DA release in BLA and no change in CA1.

VTA activity and dopamine release is correlated with salient stimuli (Kutlu et al. 2021) and lesioning the LC or VTA disinhibits the activity of the other (Guiard et al. 2008). Thus, VTA activity's influence on DA release to relevant stimuli is important to understanding the LC's role in DA release. To determine the influence of VTA on DA

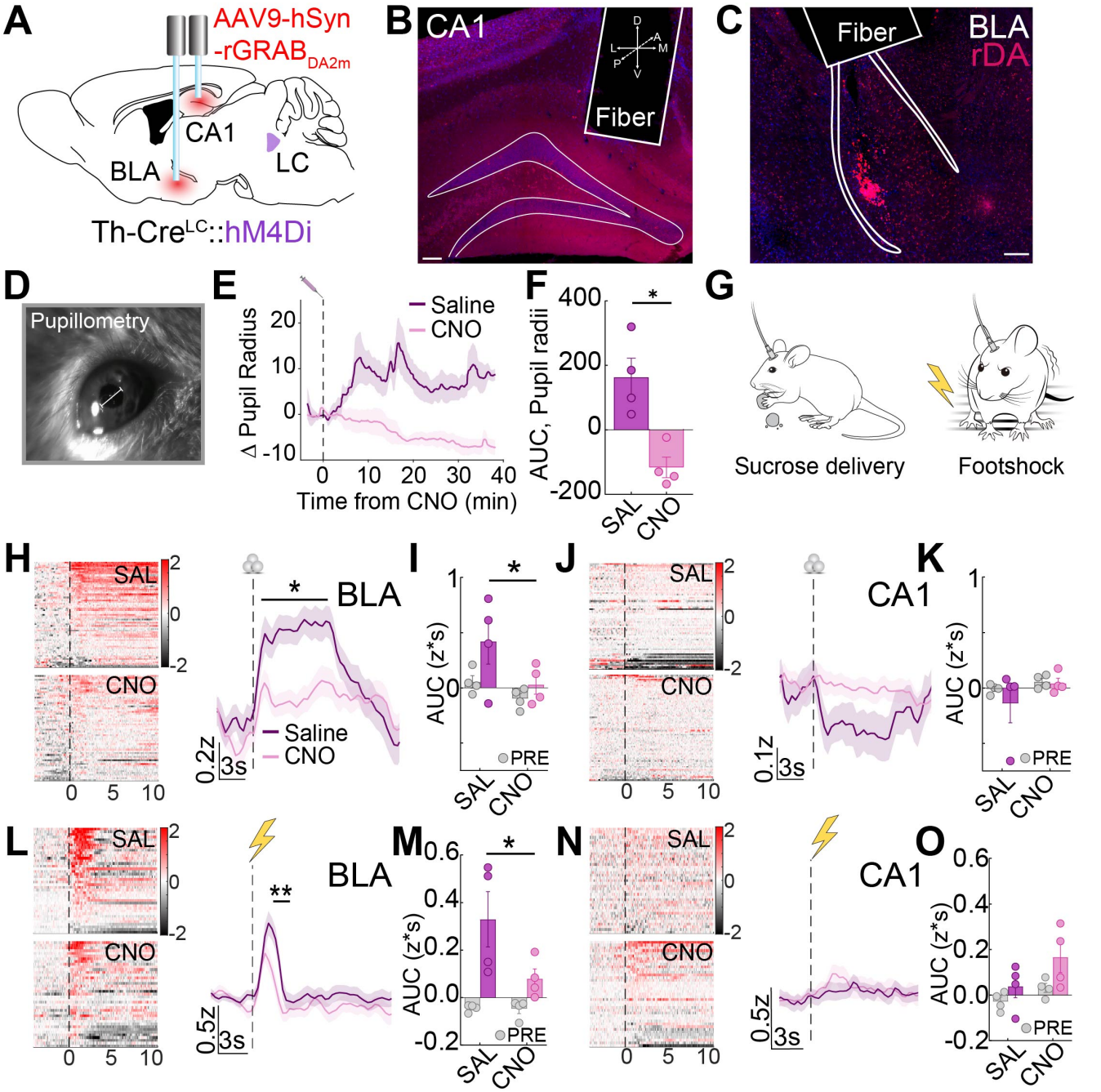

FIGURE 4 LC inhibition decreases DA release during reward and shock in BLA, and has no effect in CA1. (a) Schematic of experimental approach of surgical injections. Schematic depicts infection of LC-NE cells with Gi-DREADDs (AAV5-hSyn1-DIO-HA-hM4D(Gi)) and expression of GRAB$_{rDA2m}$ in both BLA and CA1. (b) Representative image of CA1 GRAB$_{rDA2m}$ expression and fiber placement. Scale bar, 100µm. (c) Representative image of BLA GRAB$_{rDA2m}$ expression and fiber placement. (d) Example of pupillometry recording with measurement depicted. (e) Pupil radius measurements during LC inhibition. Gi-DREADDs were expressed bilaterally in LC. n=4. (f) AUC for pupil radius measurements. (paired t-test, p=0.0223). (g) Schematic of sucrose delivery (H-K) and footshock (L-O). (h) Average traces and heatmaps for GRAB$_{rDA2m}$ response to reward retrieval in BLA during LC inhibition (pink) and saline controls (purple). Significance of 1s bins calculated using 2-way ANOVA, with Sidak test for multiple comparisons, p<0.05. n=4. (i) AUC for 10s in SAL and CNO responses to reward in BLA. 2-way ANOVA, with Sidak test for multiple comparisons, p=0.0327. (j) Average traces and heatmaps for GRAB$_{rDA2m}$ response to reward retrieval in CA1 during LC inhibition or saline. n=4. (k) AUC for 10s in SAL and CNO responses to reward in CA1. (l) Average traces and heatmaps for GRAB$_{rDA2m}$ response to shock in BLA during LC inhibition (pink) and saline (purple). Significance of 1s bins calculated using 2-way ANOVA, with Sidak test for multiple comparisons, p<0.05. n=4. (m) AUC for 5s in SAL and CNO responses to reward in BLA. 2-way ANOVA, with Sidak test for multiple comparisons, p=0.025. (n) Average traces and heatmaps for GRAB$_{rDA2m}$ response to shock in CA1 during LC inhibition or saline. n=4. (o) AUC for 5s in SAL and CNO responses to reward in CA1.

release in response to reward, we inhibited the VTA of Th-cre mice (Th-cre::VTA^{bilat}:Gi-DREADDs) as mice retrieved rewards and recorded GRAB$_{rDA2m}$ dynamics (Figure S4A). Following saline administration, DA was released in BLA during reward retrieval, and the GRAB$_{rDA2m}$ signal remained elevated during consumption (Figure S4B, left). In CA1, DA activity did not change (Figure S4B, right). In response to VTA inhibition, there was a decrease in DA that was released in the BLA during reward consumption compared to saline administration sessions, while there was no effect of this manipulation on DA activity in CA1 (Figure S4B). The latency of mice to retrieve reward was significantly increased when the VTA was inhibited (Figure S4C), establishing that the VTA's activity was suppressed by DREADD manipulation. Together, these data indicate that the LC, with the VTA, both contribute DA in the BLA during reward retrieval.

To test whether the GRAB$_{rDA2m}$ sensor is detecting NE under the same conditions, we recorded GRAB$_{rDA2m}$ and GRAB$_{NE2m}$ signal in the BLA simultaneously while mice retrieved a pellet for reward using dual-color photometry recordings. We found a clear separation in the onset of the sensors' signals (Figure S4D) that was greater than the reported on-times of the sensors (Figure 1B), suggesting these signals are likely separable and independent if carefully monitored using these considerations. Furthermore, as mice consumed reward, GRAB$_{rDA2m}$ sensor activity remained elevated for 20s after the GRAB$_{NE2m}$ activity returned to baseline. Lastly, there was no correlation between the AUC (10s post reward retrieval) of the simultaneously recorded NE and DA signals (Figure S4E). These recordings indicate we can detect separable GRAB$_{NE2m}$ and GRAB$_{rDA2m}$ signals simultaneously during freely moving behaviors, assuming sensor kinetics and transmitter release properties are divergent.

Next, we investigated the VTA's putative involvement in DA release to appetitive and aversive stimuli. Prior studies implicated DA release from LC-CA1 axons in spatial memory without VTA involvement (Kempadoo et al. 2016, Takeuchi et al. 2016), while other studies have suggested DA sourced from the VTA axon terminals modulate aversive memory acquisition independent of the LC (Tsetsenis et al. 2021). To test whether LC-sourced DA is released in response to aversive stimuli, we again used chemogenetic inhibition of LC (Th-cre::LC^{bilat}:Gi-DREADDs) prior to the delivery of an aversive footshock stimulus while recording GRAB$_{rDA2m}$ dynamics in CA1 and BLA. CNO (0.5 mg/kg, i.p.) or saline were injected 30min prior to each session, and mice received footshocks at a pseudorandom ITI of 20-90s. Following saline administration, DA was released in the BLA at the onset of a footshock, and the DA signal fell rapidly following the shock delivery. In the CA1, DA release was surprisingly not detected under the same conditions during footshock. Relative to saline treatment, inhibiting the LC-NE system during shocks produced a significant decrease in DA release in BLA during the two seconds from shock initiation (comparing 1s bins, Figure 4L, 2-way ANOVA, $p<0.01$). LC inhibition also produced a significant decrease in the GRAB$_{rDA2m}$ signal in BLA for 5s after shock onset compared to saline (Figure 4M, 2-way ANOVA, $p<0.05$). In CA1, LC inhibition had no effect on the release of DA (Figure 4N-O).

Finally, we next measured how VTA inhibition affected DA release in response to an aversive stimulus. In the BLA, DA increased with the onset of shock and returned to baseline after cessation, while in the CA1, GRAB$_{rDA2m}$ signal did not change with the shock. When the VTA was inhibited during shock sessions, there were no clear changes in the GRAB$_{rDA2m}$ signal detected in BLA or CA1 relative to saline (Figure S4F). These results indicate that VTA inhibition does not affect DA release in response to shock in both BLA and CA1 compared to saline controls, while during reward retrieval and consumption, VTA inhibition decreased DA release in the BLA compared to saline trials. Thus, only LC inhibition decreases DA release in the BLA following an aversive stimulus, suggesting that LC-NE neurons represent a major source of local DA release within the BLA during aversive stimuli.

3 | DISCUSSION

In summary, here we used optogenetics, fiber photometry and 2-photon *ex vivo* imaging to discover that stimulation and natural behavior both elicit dynamic DA release from LC terminals. We demonstrate that *in vivo*, LC-evoked NE release followed a second-order frequency response curve, while the LC-evoked DA release followed a linear trend in both BLA and CA1. We also established that LC inhibition diminished DA release in response to reward retrieval and shock in the BLA, while having minimal influence on DA release in the CA1. Together, we have established here that the LC has the capacity to release DA in both CA1 and BLA under physiologically meaningful conditions. We also determined that during appetitive and aversive stimuli, LC contributes DA release in BLA, but not appreciably in the CA1.

Recent studies have asserted that LC-NE neurons release DA in the hippocampus, enhancing contextual memory and plasticity independent of the VTA (Kempadoo et al. 2016, Smith and Greene 2012, Takeuchi et al. 2016). Some studies have used optogenetics and chemogenetics to evoke DA release from LC in dorsal CA1, but only over very long temporal domains (Kempadoo et al. 2016, Wilmot et al. 2024). In the present study we optically stimulated brain slices at much lower stimulation duration (3s), more indicative of LC-NE neuron burst activity and frequency (as low as 1hz) to determine the lower limits of physiologically-relevant LC-evoked DA and NE release. This study further characterizes LC-evoked DA release by mimicking phasic (20hz, 200ms) and tonic (5hz, 5min) activation profiles matched to physiologically relevant parameters of previously reported LC activity across mammalian species (Figure 1F, 2O-R). Although we acknowledge that optogenetic stimulation is inherently artificial, we used paradigms in this study which fall within the range of previously used and well-characterized optogenetic stimulation paradigms for LC (Carter et al. 2010, McCall 2015) actuation, which we carefully match to the natural range of LC activity (Carter et al. 2010, Devilbiss and Waterhouse 2011). In response to stimulation mimicking the natural range of LC activity, the evoked LC-NE signal followed a second-order trend while the evoked LC-DA signal followed a linear trend. These data suggest that NE and DA

release from LC terminals are regulated differently, and that there are likely differences in uptake, autoreceptor activity, metabolism, or repletion kinetics (as we recently reported) (Li et al. 2023). Future studies will need to characterize the differences in NE and DA release during various stimulation paradigms while altering transporter and vesicle activity, and also utilize FLIM-based sensor technologies, to accurately quantify these differences with higher resolution (Lee et al. 2019, Salinas et al. 2023, Zheng et al. 2025).

Additionally, in situ RNA hybridization, autoradiography and immunohistochemistry have revealed varying degrees of α1AR expression on VTA neurons (Boyajian and Loughlin 1987, Greene et al. 2005, Mitrano et al. 2012, Nicholas et al. 1993ba, Rosin et al. 1993, Solecki et al. 2022). The expression of adrenergic receptors on VTA terminals suggests LC stimulation may amplify DA release from VTA-DA terminals via a Gq-mediated effect. However, by inhibiting VTA^{TH} neurons while stimulating LC terminals, we determined that LC-evoked DA release in CA1 and BLA does not entirely rely on VTA activation (Figure 2O-2R).

While receptor pharmacology experiments have revealed the potential for DA release from noradrenergic terminals, electrical stimulation, lesions of LC, and genetic knockout of Dbh have been used to demonstrate the necessity of the LC for DA release. Selective lesioning of the LC leads to an increase in VTA-DA neuron activity, and VTA-DA lesions lead to an increase in LC-NE neuron activity (Grenhoff et al. 1993), suggesting that there are functional LC-VTA reciprocal projections (Deutch et al. 1986, Mejias-Aponte et al. 2009). These data would predict that in response to a stimulus that evokes VTA-BLA^{DA} release, the VTA may release more DA when the LC is inhibited. However, our data suggest that either LC or VTA inhibition decrease the BLA-DA release during reward retrieval (Figure 4H-I, Figure S4C). Furthermore, only LC inhibition decreased the BLA-DA release during shock (Figure 4L-M, Figure S4D), suggesting the LC's contribution of DA during an aversive stimulus may be greater than the DA released following disinhibition of VTA. Therefore, these findings taken together indicate that the LC releases DA in the BLA in response to both aversive and appetitive stimuli.

Although LC inhibition did not affect CA1-DA release in response to aversive and appetitive stimuli with $GRAB_{rDA2m}$ (Figure 4J, 4N), DA was evoked from LC terminals in CA1 through optogenetic stimulation *ex vivo* and *in vivo*. This suggests that LC-$CA1^{DA}$ release is dependent on behavioral states and neuronal activation. Because stimuli-evoked DA release decreases during LC inhibition in BLA and not CA1, but optically evoked DA release frequency response profiles do not differ significantly in these two regions (Figure 2K, 2L), LC-CA1 projections' endogenous release of DA may rely on different behavioral states than LC-BLA projections.

Recording a ligand-specific signal relies on silencing cross-reactive neuromodulator sources (e.g. VTA-DA and LC-NE neurons both project to CA1 and BLA) (López et al. 2024). To address these concerns with the biosensors used in this project, we employed genetic knockouts, inhibitory chemogenetics, and dual-color fiber photometry recordings. Through stimulating LC-$CA1^{Dbh-/-}$ projections for 3s at 20hz, there was no increase in NE signal at the upper limit of stimulation frequencies employed. In addition, $GRAB_{NE}$ and $GRAB_{DA}$ dynamics differ in response to reward retrieval and looming in CA1 (Figure 3F, S3E). This suggests that in our stimulation experiments, $GRAB_{NE}$ is sufficiently selective for NE over DA. To address concerns that the red $GRAB_{rDA2m}$ sensor used in Figure 4H-O and Figure S4B, S4D is detecting NE, we established that $GRAB_{rDA2m}$ dynamics are separable from $GRAB_{NE}$, by using dual-color fiber photometry recordings in naïve, hungry mice retrieving rewards (Figure S4C). Given the known off-kinetics of these biosensors (< 3s, Figure 1B) and the period of heightened $GRAB_{rDA2m}$ signal (>20s), $GRAB_{rDA2m}$ is likely not binding significant NE at this level of endogenous release. These data taken together suggest the $GRAB_{rDA}$ and $GRAB_{NE}$ are sufficiently selective for endogenous detection of NE and DA in these experiments.

There are also other sources of DA and NE than the LC and VTA that must also be considered herein. Studies suggest that Dorsal Raphe nucleus (DRN) has either negligible (Cho et al. 2017, Sengupta and Holmes 2019) DA innervation in BLA, and none in CA1. Substantia nigra (SN) projects to BLA, but not CA1, and these BLA projections are non-DAergic projections (Loughlin and Fallon 1983). Further studies are needed to address if the DRN or SN inputs in BLA influence the interpretation of LC-BLA^{DA} release results we report.

Past studies have suggested that DA release in BLA contributes to fear expression, primarily acquisition (Guarraci et al. 2000, Heath et al. 2015, Lamont and Kokkinidis 1998, Nader and LeDoux 1999), and that BLA-projecting VTA neurons, specifically, have been shown to release DA and contribute to conditioned fear acquisition (Tang et al. 2020). Another study demonstrated BLA projecting LC neurons contribute to fear memory formation (Uematsu et al. 2017). Our data suggest the LC is contributing some portion of DA in BLA during an aversive unconditioned stimulus (Figure 4L). Given both NE and DA are involved in fear acquisition in the amygdala (Giustino et al. 2020, Giustino and Maren 2018, Heath et al. 2015, Pantoni et al. 2020), future studies should determine how LC-sourced NE and DA released in the BLA may be involved in fear acquisition. Especially in regions with dual VTA and LC innervation, investigators focused on VTA-DA must carefully consider noradrenergic sources of DA in interpreting results.

Activity of CA1 neurons during aversive stimuli like tail shock and airpuff scales with salience and context independent of location (Barth et al. 2023), increases with the valence of a reward-predictive cue (Yun et al. 2023), and certain populations respond to reward (Gauthier and Tank 2018). While DA has been suggested to be involved in enhancing memory persistence and spatial memory (Kempadoo et al. 2016, Takeuchi et al. 2016), the present study is among the first to look at dopamine's release dynamics within CA1 during aversive and appetitive stimulus presentation. While DA was not detected in response to reward in CA1, DA release was moderately present during shock in CA1, which may be sourced from the VTA and modulating the formation of aversive memories (Tsetsenis et al. 2021). Together these data indicate that LC-CA1 projections have the capacity to release DA, but only do so under specific conditions. As hippocampal inputs to BLA

are important for contextual conditioning, CA1-DA may signal the valence of contextual information, which is then relayed to the BLA for consolidation.

While this study demonstrates the conditions for DA release from LC terminals, we do not address mechanisms of LC-DA release. DBH is not rate-limiting for NE synthesis thus how the LC may release DA has remained controversial even with emerging evidence of DA release from noradrenergic terminals. DBH is primarily localized to be inside of synaptic vesicles (Cimarusti et al. 1979) although it has also been observed less-selectively throughout the somata and processes of LC neurons (Olschowka et al. 1981), while TH is localized in the cytoplasm (Pickel et al. 1975). For DA to be released from LC neurons endogenously as the present study suggests, there must be some population of synaptic vesicles in LC terminals that do not contain DBH or whole terminals that exclude DBH-containing vesicles. Future work should use electron microscopy to explore the distribution of vesicles and DBH, and TH within LC terminals in various regions throughout the brain.

Lastly, the LC contributing DA in BLA during reward suggests there must be some active process by which DA is endogenously released from LC terminals. In some human populations, pharmacological (Gaval-Cruz and Weinshenker 2009) (e.g. disulfiram) and genetic factors (Cubells and Zabetian 2004) (e.g. *Dbh* deficiency, *Dbh* gene polymorphisms) may affect the ratio of DA/NE released by the LC, which could impact behavior especially with maladaptive comorbidities like addiction or ADHD. Due to the LC's characteristic functional differences at specific projections (Chandler et al. 2019, Uematsu et al. 2017), the impact of the corelease of DA and NE from LC axon terminal neurons on behavior identified here has large implications for the study of these two catecholamine neuromodulators across brain regions with dual VTA and LC innervation. Furthermore, understanding how these two LC-derived catecholamines function simultaneously to act on downstream GPCRs to influence neuronal activity will provide exciting insights into the fundamental neurobiology of neuromodulation and future pharmacotherapies for neuropsychiatric diseases.

REFERENCES

Ambroggi, F., Ishikawa, A., Fields, H.L. & Nicola, S.M. (2008) Basolateral amygdala neurons facilitate reward-seeking behavior by exciting nucleus accumbens neurons. *Neuron*, 59(4), 648–661. doi:10.1016/j.neuron.2008.07.004, number: 4.
URL https://www.ncbi.nlm.nih.gov/pmc/articles/PMC2603341/

Anagnostaras, S.G., Maren, S. & Fanselow, M.S. (1999) Temporally Graded Retrograde Amnesia of Contextual Fear after Hippocampal Damage in Rats: Within-Subjects Examination. *Journal of Neuroscience*, 19(3), 1106–1114. doi:10.1523/JNEUROSCI.19-03-01106.1999.
URL https://www.jneurosci.org/content/19/3/1106

Aston-Jones, G. & Cohen, J.D. (2005) AN INTEGRATIVE THEORY OF LOCUS COERULEUS-NOREPINEPHRINE FUNCTION: Adaptive Gain and Optimal Performance. *Annual Review of Neuroscience*, 28(1), 403–450. doi:10.1146/annurev.neuro.28.061604.135709, _eprint: https://doi.org/10.1146/annurev.neuro.28.061604.135709.
URL https://doi.org/10.1146/annurev.neuro.28.061604.135709

Barth, A.M., Jelitai, M., Vasarhelyi-Nagy, M.F. & Varga, V. (2023) Aversive stimulus-tuned responses in the CA1 of the dorsal hippocampus. *Nature Communications*, 14(1), 6841. doi:10.1038/s41467-023-42611-w.
URL https://www.nature.com/articles/s41467-023-42611-w

Bernacka, J., Kielbinski, M., Wawrzczak-Bargieła, A., Zajda, K., Maćkowiak, M., Przewlocki, R. et al. (2022) Alpha-2A but not 2B/C noradrenergic receptors in ventral tegmental area regulate phasic dopamine release in nucleus accumbens core. *Neuropharmacology*, 220, 109258. doi:10.1016/j.neuropharm.2022.109258.
URL https://www.sciencedirect.com/science/article/pii/S0028390822003173

Berridge, C.W. (2008) Noradrenergic modulation of arousal. *Brain Research Reviews*, 58(1), 1–17. doi:10.1016/j.brainresrev.2007.10.013.
URL https://www.sciencedirect.com/science/article/pii/S0165017307002895

Borgkvist, A., Malmlöf, T., Feltmann, K., Lindskog, M. & Schilström, B. (2011) Dopamine in the hippocampus is cleared by the norepinephrine transporter. *The International Journal of Neuropsychopharmacology*„ 1–10.doi:10.1017/S1461145711000812.
URL https://academic.oup.com/ijnp/article-lookup/doi/10.1017/S1461145711000812

Borodovitsyna, O., Flamini, M.D. & Chandler, D.J. (2018) Acute Stress Persistently Alters Locus Coeruleus Function and Anxiety-like Behavior in Adolescent Rats. *Neuroscience*, 373, 7–19. doi:10.1016/j.neuroscience.2018.01.020.
URL https://www.sciencedirect.com/science/article/pii/S0306452218300368

Bourdélat-Parks, B.N., Anderson, G.M., Donaldson, Z.R., Weiss, J.M., Bonsall, R.W., Emery, M.S. et al. (2005) Effects of dopamine β-hydroxylase genotype and disulfiram inhibition on catecholamine homeostasis in mice. *Psychopharmacology*, 183(1), 72–80. doi:10.1007/s00213-005-0139-8.
URL https://doi.org/10.1007/s00213-005-0139-8

Bouret, S. & Sara, S.J. (2004) Reward expectation, orientation of attention and locus coeruleus-medial frontal cortex interplay during learning. *European Journal of Neuroscience*, 20(3), 791–802. doi:10.1111/j.1460-9568.2004.03526.x, number: 3 _eprint: https://onlinelibrary.wiley.com/doi/pdf/10.1111/j.1460-9568.2004.03526.x.
URL https://onlinelibrary.wiley.com/doi/abs/10.1111/j.1460-9568.2004.03526.x

Boyajian, L. & Loughlin, E. (1987) Anatomical Evidence for Alpha-2 Adrenoceptor Heterogeneity: Differential Autoradiographic Distributions of [3H]Rauwolscine and [3H]Idazoxan in Rat Brain, 241.

Campeau, S. & Davis, M. (1995) Involvement of the central nucleus and basolateral complex of the amygdala in fear conditioning measured with fear-potentiated startle in rats trained concurrently with auditory and visual conditioned stimuli. *Journal of Neuroscience*, 15(3), 2301–2311. doi:10.1523/JNEUROSCI.15-03-02301.1995.
URL https://www.jneurosci.org/content/15/3/2301

Carter, M.E., Yizhar, O., Chikahisa, S., Nguyen, H., Adamantidis, A., Nishino, S. et al. (2010) Tuning arousal with optogenetic modulation of locus coeruleus neurons. *Nature Neuroscience*, 13(12), 1526–1533. doi:10.1038/nn.2682.
URL https://www.nature.com/articles/nn.2682

Chandler, D.J., Jensen, P., McCall, J.G., Pickering, A.E., Schwarz, L.A. & Totah, N.K. (2019) Redefining Noradrenergic Neuromodulation of Behavior: Impacts of a Modular Locus Coeruleus Architecture. *The Journal of Neuroscience*, 39(42), 8239–8249. doi:10.1523/JNEUROSCI.1164-19.2019, number: 42.
URL https://www.jneurosci.org/lookup/doi/10.1523/

JNEUROSCI.1164-19.2019

Chen, F.J. & Sara, S.J. (2007) Locus coeruleus activation by foot shock or electrical stimulation inhibits amygdala neurons. *Neuroscience*, 144(2), 472–481. doi:10.1016/j.neuroscience.2006.09.037.
URL https://www.sciencedirect.com/science/article/pii/S0306452206013017

Cho, J.R., Treweek, J.B., Robinson, J.E., Xiao, C., Bremner, L.R., Greenbaum, A. et al. (2017) Dorsal Raphe Dopamine Neurons Modulate Arousal and Promote Wakefulness by Salient Stimuli. *Neuron*, 94(6), 1205–1219.e8. doi:10.1016/j.neuron.2017.05.020.
URL https://www.cell.com/neuron/abstract/S0896-6273(17)30458-0

Cimarusti, D.L., Saito, K., Vaughn, J.E., Barber, R., Roberts, E. & Thomas, P.E. (1979) Immunocytochemical localization of dopamine-β-hydroxylase in rat locus coeruleus and hypothalamus. *Brain Research*, 162(1), 55–67. doi:10.1016/0006-8993(79)90755-8.
URL https://www.sciencedirect.com/science/article/pii/0006899379907558

Cubells, J.F., Kranzler, H.R., McCance-Katz, E., Anderson, G.M., Malison, R.T., Price, L.H. et al. (2000) A haplotype at the DBH locus, associated with low plasma dopamine β-hydroxylase activity, also associates with cocaine-induced paranoia. *Molecular Psychiatry*, 5(1), 56–63. doi:10.1038/sj.mp.4000657.
URL https://www.nature.com/articles/4000657

Cubells, J.F. & Zabetian, C.P. (2004) Human genetics of plasma dopamine beta-hydroxylase activity: applications to research in psychiatry and neurology. *Psychopharmacology*, 174(4), 463–476. doi:10.1007/s00213-004-1840-8.

Curtis, A.L., Leiser, S.C., Snyder, K. & Valentino, R.J. (2012) Predator stress engages corticotropin-releasing factor and opioid systems to alter the operating mode of locus coeruleus norepinephrine neurons. *Neuropharmacology*, 62(4), 1737–1745. doi:10.1016/j.neuropharm.2011.11.020, number: 4.
URL https://www.sciencedirect.com/science/article/pii/S0028390811004990

Davis, M. & Whalen, P.J. (2001) The amygdala: vigilance and emotion. *Molecular Psychiatry*, 6(1), 13–34. doi:10.1038/sj.mp.4000812.
URL https://www.nature.com/articles/4000812

de Medeiros, M.A., Carlos Reis, L. & Eugênio Mello, L. (2005) Stress-Induced c-Fos Expression is Differentially Modulated by Dexamethasone, Diazepam and Imipramine. *Neuropsychopharmacology*, 30(7), 1246–1256. doi:10.1038/sj.npp.1300694, bandiera_abtest: a Cg_type: Nature Research Journals Number: 7 Primary_atype: Research.
URL https://www.nature.com/articles/1300694

Deutch, A.Y., Goldstein, M. & Roth, R.H. (1986) Activation of the locus coeruleus induced by selective stimulation of the ventral tegmental area. *Brain Research*, 363(2), 307–314. doi:10.1016/0006-8993(86)91016-4.
URL https://www.sciencedirect.com/science/article/pii/0006899386910164

Devilbiss, D.M. & Waterhouse, B.D. (2011) Phasic and Tonic Patterns of Locus Coeruleus Output Differentially Modulate Sensory Network Function in the Awake Rat. *Journal of Neurophysiology*, 105(1), 69–87. doi:10.1152/jn.00445.2010, number: 1.
URL https://www.ncbi.nlm.nih.gov/pmc/articles/PMC3023368/

Devoto, P., Flore, G., Longu, G., Pira, L. & Gessa, G.L. (2003) Origin of extracellular dopamine from dopamine and noradrenaline neurons in the medial prefrontal and occipital cortex. *Synapse*, 50(3), 200–205. doi:10.1002/syn.10264, _eprint: https://onlinelibrary.wiley.com/doi/pdf/10.1002/syn.10264.
URL https://onlinelibrary.wiley.com/doi/abs/10.1002/syn.10264

Devoto, P., Flore, G., Pira, L., Longu, G. & Gessa, G.L. (2004) Alpha2-adrenoceptor mediated co-release of dopamine and noradrenaline from noradrenergic neurons in the cerebral cortex. *Journal of Neurochemistry*, 88(4), 1003–1009. doi:10.1046/j.1471-4159.2003.02239.x, _eprint: https://onlinelibrary.wiley.com/doi/pdf/10.1046/j.1471-4159.2003.02239.x.
URL https://onlinelibrary.wiley.com/doi/abs/10.1046/j.1471-4159.2003.02239.x

Devoto, P., Flore, G., Saba, P., Fa, M. & Gessa, G.L. (2005) Stimulation of the locus coeruleus elicits noradrenaline and dopamine release in the medial prefrontal and parietal cortex. *Journal of Neurochemistry*, 92(2), 368–374. doi:10.1111/j.1471-4159.2004.02866.x, number: 2.
URL http://doi.wiley.com/10.1111/j.1471-4159.2004.02866.x

Devoto, P., Flore, G., Saba, P., Fà, M. & Gessa, G. (2005) Co-release of noradrenaline and dopamine in the cerebral cortex elicited by single train and repeated train stimulation of the locus coeruleus. *BMC Neuroscience*, 6(1), 31. doi:10.1186/1471-2202-6-31, number: 1.
URL http://bmcneurosci.biomedcentral.com/articles/10.1186/1471-2202-6-31

Dupret, D., O'Neill, J., Pleydell-Bouverie, B. & Csicsvari, J. (2010) The reorganization and reactivation of hippocampal maps predict spatial memory performance. *Nature Neuroscience*, 13(8), 995–1002. doi:10.1038/nn.2599, bandiera_abtest: a Cg_type: Nature Research Journals Number: 8 Primary_atype: Research Subject_term: Learning and memory;Neuronal physiology;Sleep Subject_term_id: learning-and-memory;neuronal-physiology;sleep.
URL https://www.nature.com/articles/nn.2599

Fanselow, M.S. & LeDoux, J.E. (1999) Why We Think Plasticity Underlying Pavlovian Fear Conditioning Occurs in the Basolateral Amygdala. *Neuron*, 23(2), 229–232. doi:10.1016/S0896-6273(00)80775-8, number: 2.
URL https://www.cell.com/neuron/abstract/S0896-6273(00)80775-8

Feng, J., Dong, H., Lischinsky, J.E., Zhou, J., Deng, F., Zhuang, C. et al. (2024) Monitoring norepinephrine release in vivo using next-generation GRABNE sensors. *Neuron*, 112(12), 1930–1942.e6. doi:10.1016/j.neuron.2024.03.001.
URL https://linkinghub.elsevier.com/retrieve/pii/S0896627324001557

Feng, J., Zhang, C., Lischinsky, J.E., Jing, M., Zhou, J., Wang, H. et al. (2019) A Genetically Encoded Fluorescent Sensor for Rapid and Specific In Vivo Detection of Norepinephrine. *Neuron*, 102(4), 745–761.e8. doi:10.1016/j.neuron.2019.02.037, number: 4.
URL https://linkinghub.elsevier.com/retrieve/pii/S0896627319301722

Gauthier, J.L. & Tank, D.W. (2018) A Dedicated Population for Reward Coding in the Hippocampus. *Neuron*, 99(1), 179–193.e7. doi:10.1016/j.neuron.2018.06.008.
URL https://www.sciencedirect.com/science/article/pii/S0896627318304768

Gaval-Cruz, M. & Weinshenker, D. (2009) mechanisms of disulfiram-induced cocaine abstinence: antabuse and cocaine relapse. *Molecular Interventions*, 9(4), 175–187. doi:10.1124/mi.9.4.6.

Giustino, T.F. & Maren, S. (2018) Noradrenergic Modulation of Fear Conditioning and Extinction. *Frontiers in Behavioral Neuroscience*, 12, 43. doi:10.3389/fnbeh.2018.00043.
URL https://www.ncbi.nlm.nih.gov/pmc/articles/PMC5859179/

Giustino, T.F., Ramanathan, K.R., Totty, M.S., Miles, O.W. & Maren, S. (2020) Locus Coeruleus Norepinephrine Drives Stress-Induced Increases in Basolateral Amygdala Firing and Impairs Extinction Learning. *The Journal of Neuroscience*, 40(4), 907–916. doi:10.1523/JNEUROSCI.1092-19.2019, number: 4.

URL https://www.jneurosci.org/lookup/doi/10.1523/JNEUROSCI.1092-19.2019

Greene, J.G., Dingledine, R. & Greenamyre, J.T. (2005) Gene expression profiling of rat midbrain dopamine neurons: implications for selective vulnerability in parkinsonism. *Neurobiology of Disease*, 18(1), 19–31. doi:10.1016/j.nbd.2004.10.003.
URL https://www.sciencedirect.com/science/article/pii/S0969996104002360

Grenhoff, J., Nisell, M., Ferré, S., Aston-Jones, G. & Svensson, T.H. (1993) Noradrenergic modulation of midbrain dopamine cell firing elicited by stimulation of the locus coeruleus in the rat. *Journal of Neural Transmission / General Section JNT*, 93(1), 11–25. doi:10.1007/BF01244934.
URL https://doi.org/10.1007/BF01244934

Grimm, C., Duss, S.N., Privitera, M., Munn, B.R., Karalis, N., Frässle, S. et al. (2024) Tonic and burst-like locus coeruleus stimulation distinctly shift network activity across the cortical hierarchy. *Nature Neuroscience*, 27(11), 2167–2177. doi:10.1038/s41593-024-01755-8.
URL https://www.nature.com/articles/s41593-024-01755-8

Guarraci, F.A., Frohardt, R.J., Falls, W.A. & Kapp, B.S. (2000) The effects of intra-amygdaloid infusions of a D_2 dopamine receptor antagonist on Pavlovian fear conditioning. *Behavioral Neuroscience*, 114(3), 647–651. doi:10.1037/0735-7044.114.3.647, place: US.

Guiard, B.P., El Mansari, M., Merali, Z. & Blier, P. (2008) Functional interactions between dopamine, serotonin and norepinephrine neurons: an in-vivo electrophysiological study in rats with monoaminergic lesions. *International Journal of Neuropsychopharmacology*, 11(5), 625–639. doi:10.1017/S1461145707008383.
URL https://doi.org/10.1017/S1461145707008383

Gálvez-Márquez, D.K., Salgado-Ménez, M., Moreno-Castilla, P., Rodríguez-Durán, L., Escobar, M.L., Tecuapetla, F. et al. (2022) Spatial contextual recognition memory updating is modulated by dopamine release in the dorsal hippocampus from the locus coeruleus. *Proceedings of the National Academy of Sciences*, 119(49), e2208254119. doi:10.1073/pnas.2208254119.
URL https://www.pnas.org/doi/full/10.1073/pnas.2208254119

Hauber, W. (1996) Impairments of movement initiation and execution induced by a blockade of dopamine D1 OR D2 receptors are reversed by a blockade of *N*-methyl-d-aspartate receptors. *Neuroscience*, 73(1), 121–130. doi:10.1016/0306-4522(96)00036-X.
URL https://www.sciencedirect.com/science/article/pii/030645229600036X

Heath, F.C., Jurkus, R., Bast, T., Pezze, M.A., Lee, J.L.C., Voigt, J.P. et al. (2015) Dopamine D1-like receptor signalling in the hippocampus and amygdala modulates the acquisition of contextual fear conditioning. *Psychopharmacology*, 232(14), 2619–2629. doi:10.1007/s00213-015-3897-y, number: 14.
URL http://link.springer.com/10.1007/s00213-015-3897-y

Kaufman, A.M., Geiller, T. & Losonczy, A. (2020) A Role for the Locus Coeruleus in Hippocampal CA1 Place Cell Reorganization during Spatial Reward Learning. *Neuron*, 105(6), 1018–1026.e4. doi:10.1016/j.neuron.2019.12.029, number: 6.
URL https://linkinghub.elsevier.com/retrieve/pii/S0896627319310955

Kelberman, M.A., Rodberg, E., Arabzadeh, E., Bair-Marshall, C.J., Berridge, C.W., Berrocoso, E. et al. (2024) Diversity of ancestral brainstem noradrenergic neurons across species and multiple biological factors. *bioRxiv*„ 2024.10.14.618224.doi:10.1101/2024.10.14.618224.
URL https://www.ncbi.nlm.nih.gov/pmc/articles/PMC11507722/

Kempadoo, K.A., Mosharov, E.V., Choi, S.J., Sulzer, D. & Kandel, E.R. (2016) Dopamine release from the locus coeruleus to the dorsal hippocampus promotes spatial learning and memory. *Proceedings of the National Academy of Sciences*, 113(51), 14835–14840. doi:10.1073/pnas.1616515114, number: 51.
URL http://www.pnas.org/lookup/doi/10.1073/pnas.1616515114

Koob, G.F., Balcom, G.J. & Meyerhoff, J.L. (1975) Dopamine and norepinephrine levels in the nucleus accumbens, olfactory tubercle and corpus striatum following lesions in the ventral tegmental area. *Brain Research*, 94(1), 45–55. doi:10.1016/0006-8993(75)90875-6.
URL https://www.sciencedirect.com/science/article/pii/0006899375908756

Kutlu, M.G., Zachry, J.E., Melugin, P.R., Cajigas, S.A., Chevee, M.F., Kelly, S.J. et al. (2021) Dopamine release in the nucleus accumbens core signals perceived saliency. *Current Biology*, 31(21), 4748–4761.e8. doi:10.1016/j.cub.2021.08.052.
URL https://www.sciencedirect.com/science/article/pii/S096098222101188X

Lamont, E.W. & Kokkinidis, L. (1998) Infusion of the dopamine D1 receptor antagonist SCH 23390 into the amygdala blocks fear expression in a potentiated startle paradigm. *Brain Research*, 795(1), 128–136. doi:10.1016/S0006-8993(98)00281-9.
URL https://www.sciencedirect.com/science/article/pii/S0006899398002819

Lee, S.J., Chen, Y., Lodder, B. & Sabatini, B.L. (2019) Monitoring Behaviorally Induced Biochemical Changes Using Fluorescence Lifetime Photometry. *Frontiers in Neuroscience*, 13. doi:10.3389/fnins.2019.00766.
URL https://www.frontiersin.org/journals/neuroscience/articles/10.3389/fnins.2019.00766/full

Li, L., Rana, A.N., Li, E.M., Feng, J., Li, Y. & Bruchas, M.R. (2023) Activity-dependent constraints on catecholamine signaling. *Cell Reports*, 42(12). doi:10.1016/j.celrep.2023.113566.
URL https://www.cell.com/cell-reports/abstract/S2211-1247(23)01578-4

Lieberman, A., Freedman, L. & Goldstein, M. (1972) SERUM DOPAMINE-β-HYDROXYLASE ACTIVITY IN PATIENTS WITH HUNTINGTON'S CHOREA AND PARKINSON'S DISEASE. *The Lancet*, 299(7742), 153–154. doi:10.1016/S0140-6736(72)90725-8.
URL https://www.sciencedirect.com/science/article/pii/S0140673672907258

Lisman, J.E. & Grace, A.A. (2005) The Hippocampal-VTA Loop: Controlling the Entry of Information into Long-Term Memory. *Neuron*, 46(5), 703–713. doi:10.1016/j.neuron.2005.05.002, number: 5.
URL https://www.sciencedirect.com/science/article/pii/S0896627305003971

Liu, J., Lin, L. & Wang, D.V. (2021) Representation of Fear of Heights by Basolateral Amygdala Neurons. *Journal of Neuroscience*, 41(5), 1080–1091. doi:10.1523/JNEUROSCI.0483-20.2020.
URL https://www.jneurosci.org/content/41/5/1080

Loughlin, S.E. & Fallon, J.H. (1983) Dopaminergic and non-dopaminergic projections to amygdala from substantia nigra and ventral tegmental area. *Brain Research*, 262(2), 334–338. doi:10.1016/0006-8993(83)91029-6.
URL https://www.sciencedirect.com/science/article/pii/0006899383910296

López, R.C., Noble, N., Özçete, ̇.D., Cai, X., Handy, G.E., Andersen, J.W. et al. (2024) *Innervation density governs crosstalk of GPCR-based norepinephrine and dopamine sensors*. Pages: 2024.11.23.624963 Section: New Results.
URL https://www.biorxiv.org/content/10.1101/2024.11.23.624963v1

Maren, S. (2001) Neurobiology of Pavlovian Fear Conditioning. *Annual Review of Neuroscience*, 24(Volume 24, 2001), 897–931. doi:10.1146/annurev.neuro.24.1.897.
URL https://www.annualreviews.org/content/journals/10.1146/annurev.neuro.24.1.897

Maren, S., De Oca, B. & Fanselow, M.S. (1994) Sex differences in hippocampal long-term potentiation (LTP) and Pavlovian fear con-

ditioning in rats: positive correlation between LTP and contextual learning. *Brain Research*, 661(1), 25–34. doi:10.1016/0006-8993(94)91176-2, number: 1.
URL https://www.sciencedirect.com/science/article/pii/0006899394911762

Martig, A.K. & Mizumori, S.J.Y. (2011) Ventral tegmental area disruption selectively affects CA1/CA2 but not CA3 place fields during a differential reward working memory task. *Hippocampus*, 21(2), 172–184. doi:10.1002/hipo.20734, number: 2.

McCall, J.G. (2015) CRH Engagement of the Locus Coeruleus Noradrenergic System Mediates Stress-Induced Anxiety„ 36.

McCall, J.G., Siuda, E.R., Bhatti, D.L., Lawson, L.A., McElligott, Z.A., Stuber, G.D. et al. (2017) Locus coeruleus to basolateral amygdala noradrenergic projections promote anxiety-like behavior. *eLife*, 6, e18247. doi:10.7554/eLife.18247.
URL https://elifesciences.org/articles/18247

Mejias-Aponte, C.A., Drouin, C. & Aston-Jones, G. (2009) Adrenergic and Noradrenergic Innervation of the Midbrain Ventral Tegmental Area and Retrorubral Field: Prominent Inputs from Medullary Homeostatic Centers. *Journal of Neuroscience*, 29(11), 3613–3626. doi:10.1523/JNEUROSCI.4632-08.2009.
URL https://www.jneurosci.org/lookup/doi/10.1523/JNEUROSCI.4632-08.2009

Meltzer, H.Y., Cho, H.W. & Carroll, B.J. (1976) Serum Dopamine-βHydroxylase Activity in the Affective Psychoses and Schizophrenia: Decreased Activity in Unipolar Psychotically Depressed Patients. *Archives of General Psychiatry*, 33(5), 585–591. doi:10.1001/archpsyc.1976.01770050047007.
URL https://doi.org/10.1001/archpsyc.1976.01770050047007

Millard, S.J., Hoang, I.B., Sherwood, S., Taira, M., Reyes, V., Greer, Z. et al. (2024) Cognitive representations of intracranial self-stimulation of midbrain dopamine neurons depend on stimulation frequency. *Nature Neuroscience*, 27(7), 1253–1259. doi:10.1038/s41593-024-01643-1.
URL https://www.nature.com/articles/s41593-024-01643-1

Mitrano, D.A., Schroeder, J.P., Smith, Y., Cortright, J.J., Bubula, N., Vezina, P. et al. (2012) Alpha-1 Adrenergic Receptors are Localized on Presynaptic Elements in the Nucleus Accumbens and Regulate Mesolimbic Dopamine Transmission. *Neuropsychopharmacology*, 37(9), 2161–2172. doi:10.1038/npp.2012.68.
URL https://www.ncbi.nlm.nih.gov/pmc/articles/PMC3398716/

Nader, K. & LeDoux, J. (1999) Inhibition of the mesoamygdala dopaminergic pathway impairs the retrieval of conditioned fear associations. *Behavioral Neuroscience*, 113(5), 891–901. doi:10.1037/0735-7044.113.5.891, place: US.

Nagatsu, T., Wakui, Y., Kato, T., Fujita, K., Kondo, T., Yokochi, F. et al. (1982) **Dopamine beta-hydroxylase activity in cerebrospinal fluid of Parkinsonian patients** . *Biomedical Research*, 3(1), 95–98. doi:10.2220/biomedres.3.95.
URL https://www.jstage.jst.go.jp/article/biomedres/3/1/3_95/_article

Nakahara, H., Itoh, H., Kawagoe, R., Takikawa, Y. & Hikosaka, O. (2004) Dopamine Neurons Can Represent Context-Dependent Prediction Error. *Neuron*, 41(2), 269–280. doi:10.1016/S0896-6273(03)00869-9, number: 2.
URL https://www.sciencedirect.com/science/article/pii/S0896627303008699

Nicholas, A.P., Pieribone, V. & Hökfelt, T. (1993) Distributions of mRNAs for alpha-2 adrenergic receptor subtypes in rat brain: An in situ hybridization study. *Journal of Comparative Neurology*, 328(4), 575–594. doi:10.1002/cne.903280409, _eprint: https://onlinelibrary.wiley.com/doi/pdf/10.1002/cne.903280409.
URL https://onlinelibrary.wiley.com/doi/abs/10.1002/cne.903280409

Nicholas, A.P., Pieribone, V.A. & Hökfelt, T. (1993) Cellular localization of messenger RNA for beta-1 and beta-2 adrenergic receptors in rat brain: An in situ hybridization study. *Neuroscience*, 56(4), 1023–1039. doi:10.1016/0306-4522(93)90148-9.
URL https://www.sciencedirect.com/science/article/pii/0306452293901489

Olschowka, J.A., Molliver, M.E., Grzanna, R., Rice, F.L. & Coyle, J.T. (1981) Ultrastructural demonstration of noradrenergic synapses in the rat central nervous system by dopamine-beta-hydroxylase immunocytochemistry. *The Journal of Histochemistry and Cytochemistry: Official Journal of the Histochemistry Society*, 29(2), 271–280. doi:10.1177/29.2.7019303.

Pantoni, M.M., Carmack, S.A., Hammam, L. & Anagnostaras, S.G. (2020) Dopamine and norepinephrine transporter inhibition for long-term fear memory enhancement. *Behavioural Brain Research*, 378, 112266. doi:10.1016/j.bbr.2019.112266.

Paton, J.J., Belova, M.A., Morrison, S.E. & Salzman, C.D. (2006) The primate amygdala represents the positive and negative value of visual stimuli during learning. *Nature*, 439(7078), 865–870. doi:10.1038/nature04490.
URL https://www.nature.com/articles/nature04490

Patriarchi, T., Cho, J.R., Merten, K., Howe, M.W., Marley, A., Xiong, W.H. et al. (2018) Ultrafast neuronal imaging of dopamine dynamics with designed genetically encoded sensors. *Science*, 360(6396), eaat4422. doi:10.1126/science.aat4422, number: 6396.
URL https://www.sciencemag.org/lookup/doi/10.1126/science.aat4422

Phillips, R.G. & LeDoux, J.E. (1992) Differential contribution of amygdala and hippocampus to cued and contextual fear conditioning. *Behavioral Neuroscience*, 106(2), 274–285. doi:10.1037/0735-7044.106.2.274, place: US.

Pickel, V.M., Joh, T.H. & Reis, D.J. (1975) Ultrastructural localization of tyrosine hydroxylase in noradrenergic neurons of brain. *Proceedings of the National Academy of Sciences*, 72(2), 659–663. doi:10.1073/pnas.72.2.659.
URL https://www.pnas.org/doi/abs/10.1073/pnas.72.2.659

Poe, G.R., Foote, S., Eschenko, O., Johansen, J.P., Bouret, S., Aston-Jones, G. et al. (2020) Locus coeruleus: a new look at the blue spot. *Nature Reviews Neuroscience*, 21(11), 644–659. doi:10.1038/s41583-020-0360-9, number: 11.
URL https://www.nature.com/articles/s41583-020-0360-9

Privitera, M., Ferrari, K.D., von Ziegler, L.M., Sturman, O., Duss, S.N., Floriou-Servou, A. et al. (2020) A complete pupillometry toolbox for real-time monitoring of locus coeruleus activity in rodents. *Nature Protocols*, 15(8), 2301–2320. doi:10.1038/s41596-020-0324-6.
URL https://www.nature.com/articles/s41596-020-0324-6

Privitera, M., Ziegler, L.M.v., Floriou-Servou, A., Duss, S.N., Zhang, R., Waag, R. et al. (2024) Noradrenaline release from the locus coeruleus shapes stress-induced hippocampal gene expression. *eLife*, 12. doi:10.7554/eLife.88559.2.
URL https://elifesciences.org/reviewed-preprints/88559

Rosin, D.L., Zeng, D., Stornetta, R.L., Norton, F.R., Riley, T., Okusa, M.D. et al. (1993) Immunohistochemical localization ofα2a-adrenergic receptors in catecholaminergic and other brainstem neurons in the rat. *Neuroscience*, 56(1), 139–155. doi:10.1016/0306-4522(93)90569-2.
URL https://www.sciencedirect.com/science/article/pii/0306452293905692

Salinas, A.G., Lee, J.O., Augustin, S.M., Zhang, S., Patriarchi, T., Tian, L. et al. (2023) Distinct sub-second dopamine signaling in dorsolateral striatum measured by a genetically-encoded fluorescent sensor. *Nature Communications*, 14(1), 5915. doi:10.1038/s41467-023-41581-3.
URL https://www.nature.com/articles/s41467-023-41581-3

Schoenbaum, G., Chiba, A.A. & Gallagher, M. (1999) Neural Encoding in Orbitofrontal Cortex and Basolateral Amygdala during Olfactory Discrimination Learning. *Journal of Neuroscience*, 19(5),

1876–1884. doi:10.1523/JNEUROSCI.19-05-01876.1999.
URL https://www.jneurosci.org/content/19/5/1876

Sengupta, A. & Holmes, A. (2019) A Discrete Dorsal Raphe to Basal Amygdala 5-HT Circuit Calibrates Aversive Memory. *Neuron*, 103(3), 489–505.e7. doi:10.1016/j.neuron.2019.05.029.
URL https://www.cell.com/neuron/abstract/S0896-6273(19)30482-9

Seo, D.O., Zhang, E.T., Piantadosi, S.C., Marcus, D.J., Motard, L.E., Kan, B.K. et al. (2021) A locus coeruleus to dentate gyrus noradrenergic circuit modulates aversive contextual processing. *Neuron*, 109(13), 2116–2130.e6. doi:10.1016/j.neuron.2021.05.006, number: 13.

Shukla, A. & Chattarji, S. (2022) Stressed rats fail to exhibit avoidance reactions to innately aversive social calls. *Neuropsychopharmacology*, 47(6), 1145–1155. doi:10.1038/s41386-021-01230-z.
URL https://www.nature.com/articles/s41386-021-01230-z

Silveira, M.C.L., Sandner, G. & Graeff, F.G. (1993) Induction of Fos immunoreactivity in the brain by exposure to the elevated plus-maze. *Behavioural Brain Research*, 56(1), 115–118. doi:10.1016/0166-4328(93)90028-O, number: 1.
URL https://www.sciencedirect.com/science/article/pii/0166432893900028O

Sinha, R., Catapano, D. & O'Malley, S. (1999) Stress-induced craving and stress response in cocaine dependent individuals. *Psychopharmacology*, 142(4), 343–351. doi:10.1007/s002130050898, number: 4.
URL https://doi.org/10.1007/s002130050898

Smith, C.C. & Greene, R.W. (2012) CNS Dopamine Transmission Mediated by Noradrenergic Innervation. *Journal of Neuroscience*, 32(18), 6072–6080. doi:10.1523/JNEUROSCI.6486-11.2012, number: 18.
URL https://www.jneurosci.org/lookup/doi/10.1523/JNEUROSCI.6486-11.2012

Solecki, W.B., Kielbinski, M., Bernacka, J., Gralec, K., Klasa, A., Pradel, K. et al. (2022) Alpha1-adrenergic receptor blockade in the ventral tegmental area attenuates acquisition of cocaine-induced pavlovian associative learning. *Frontiers in Behavioral Neuroscience*, 16, 969104. doi:10.3389/fnbeh.2022.969104.

Sun, F., Zhou, J., Dai, B., Qian, T., Zeng, J., Li, X. et al. (2020) Next-generation GRAB sensors for monitoring dopaminergic activity in vivo. *Nature Methods*, 17(11), 1156–1166. doi:10.1038/s41592-020-00981-9, number: 11.
URL http://www.nature.com/articles/s41592-020-00981-9

Szot, P., Weinshenker, D., White, S.S., Robbins, C.A., Rust, N.C., Schwartzkroin, P.A. et al. (1999) Norepinephrine-Deficient Mice Have Increased Susceptibility to Seizure-Inducing Stimuli. *Journal of Neuroscience*, 19(24), 10985–10992. doi:10.1523/JNEUROSCI.19-24-10985.1999.
URL https://www.jneurosci.org/content/19/24/10985

Takeuchi, T., Duszkiewicz, A.J., Sonneborn, A., Spooner, P.A., Yamasaki, M., Watanabe, M. et al. (2016) Locus coeruleus and dopaminergic consolidation of everyday memory. *Nature*, 537(7620), 357–362. doi:10.1038/nature19325, number: 7620.
URL http://www.nature.com/articles/nature19325

Tang, W., Kochubey, O., Kintscher, M. & Schneggenburger, R. (2020) A VTA to Basal Amygdala Dopamine Projection Contributes to Signal Salient Somatosensory Events during Fear Learning. *Journal of Neuroscience*, 40(20), 3969–3980. Number: 20.

Thomas, S.A., Marck, B.T., Palmiter, R.D. & Matsumoto, A.M. (1998) Restoration of norepinephrine and reversal of phenotypes in mice lacking dopamine beta-hydroxylase. *Journal of Neurochemistry*, 70(6), 2468–2476. doi:10.1046/j.1471-4159.1998.70062468.x.

Thomas, S.A., Matsumoto, A.M. & Palmiter, R.D. (1995) Noradrenaline is essential for mouse fetal development. *Nature*, 374(6523), 643–646. doi:10.1038/374643a0.
URL https://www.nature.com/articles/374643a0

Tsetsenis, T., Badyna, J.K., Wilson, J.A., Zhang, X., Krizman, E.N., Subramaniyan, M. et al. (2021) Midbrain dopaminergic innervation of the hippocampus is sufficient to modulate formation of aversive memories. *Proceedings of the National Academy of Sciences*, 118(40), e2111069118. doi:10.1073/pnas.2111069118.
URL https://www.pnas.org/doi/10.1073/pnas.2111069118

Tye, K.M. & Janak, P.H. (2007) Amygdala Neurons Differentially Encode Motivation and Reinforcement. *Journal of Neuroscience*, 27(15), 3937–3945. doi:10.1523/JNEUROSCI.5281-06.2007.
URL https://www.jneurosci.org/content/27/15/3937

Uematsu, A., Tan, B.Z., Ycu, E.A., Cuevas, J.S., Koivumaa, J., Junyent, F. et al. (2017) Modular organization of the brainstem noradrenaline system coordinates opposing learning states. *Nature Neuroscience*, 20(11), 1602–1611. doi:10.1038/nn.4642, number: 11.
URL http://www.nature.com/articles/nn.4642

Uwano, T., Nishijo, H., Ono, T. & Tamura, R. (1995) Neuronal responsiveness to various sensory stimuli, and associative learning in the rat amygdala. *Neuroscience*, 68(2), 339–361. doi:10.1016/0306-4522(95)00125-3.
URL https://www.sciencedirect.com/science/article/pii/0306452295001253

Wilmot, J.H., Diniz, C.R.A.F., Crestani, A.P., Puhger, K.R., Roshgadol, J., Tian, L. et al. (2024) Phasic locus coeruleus activity enhances trace fear conditioning by increasing dopamine release in the hippocampus. *eLife*, 12, RP91465. doi:10.7554/eLife.91465.

Yamamoto, K., Cubells, J.F., Gelernter, J., Benkelfat, C., Lalonde, P., Bloom, D. et al. (2003) Dopamine Beta-Hydroxylase (DBH) gene and schizophrenia phenotypic variability: A genetic association study. *American Journal of Medical Genetics Part B: Neuropsychiatric Genetics*, 117B(1), 33–38. doi:10.1002/ajmg.b.10011, _eprint: https://onlinelibrary.wiley.com/doi/pdf/10.1002/ajmg.b.10011.
URL https://onlinelibrary.wiley.com/doi/abs/10.1002/ajmg.b.10011

Yun, M., Hwang, J.Y. & Jung, M.W. (2023) Septotemporal variations in hippocampal value and outcome processing. *Cell Reports*, 42(2). doi:10.1016/j.celrep.2023.112094.
URL https://www.cell.com/cell-reports/abstract/S2211-1247(23)00105-5

Zheng, Y., Cai, R., Wang, K., Zhang, J., Zhuo, Y., Dong, H. et al. (2025) In vivo multiplex imaging of dynamic neurochemical networks with designed far-red dopamine sensors. *Science*, 388(6751), eadt7705. doi:10.1126/science.adt7705.
URL https://www.science.org/doi/10.1126/science.adt7705

4 | METHODS

Animals

Adult (20-35 g) male or female *Dbh*-cre or *Th*-cre mice and Cre (-) littermate control mice were used for *in vivo* experiments after backcrossing to C57BL/6J mice for at least 10 generations. Mice were group housed, given access to food pellets and water ad libitum, and maintained on a 12:12-hour dark/light cycle (lights off at 7:00 a.m.). Animals were held in a sound attenuated holding room facility in the lab starting at least one week prior to surgery, as well as post-surgery and throughout the duration of behavioral assays to minimize stress from transportation and disruption from foot traffic. All mice were handled and, where appropriate, connected to fiber optics two times a day for one week prior to behavioral experimental testing. All experimental procedures were approved by the Animal Care and Use Committee of Washington University and the Animal Care and Use Committee of University of Washington and conformed to NIH guidelines.

Stereotaxic surgery

Surgeries were performed under 2% isoflurane anesthesia (Piramal Healthcare, Maharashtra, India). All injections in BLA and CA1 were done using a Hamilton blunt syringe (Reno, NV), while injections into the LC were completed using a Hamilton beveled syringe (Reno, NV).

For detecting NE and DA dynamics in ex-vivo slice experiments, Dbh-cre mice were injected with 500nL of AAV1-hSyn-GRAB$_{NE2m}$-eGFP or AAV2/9-hSyn-WPRE-PA-GRAB$_{DA3m}$-eGFP into dorsal CA1 (AP: 1.9, ML: -1.4, DV: -1.65) (Dbh-cre::BLA or CA1: GRAB$_{DA}$ or GRAB$_{NE}$). To activate terminals while recording, Chrimson was injected into the LC (AP: -5.45, ML: -1.10, DV: -4.3 to -3.9) of the same mice (Dbh-cre::LC:Chrimson). Mice were allowed to recover and viruses to express for a minimum of 5 weeks.

For recording initial neural dynamics in response to behaviors, either 500nL of AAV2/9-hSyn-WPRE-PA-GRAB$_{DA3m}$-eGFP or AAV1-hSyn-GRAB$_{NE2m}$ (both prepared in the UW NAPE center Viral Core, Seattle, WA) were injected with a Hamilton blunt syringe (Reno, NV) into the BLA (AP: -1.4, ML: -3.15, DV: -4.8 to -4.55), dCA1 (AP: 1.9, ML: -1.4, DV: -1.65) of Dbh-cre mice (Dbh-cre::BLA or CA1:GRAB$_{DA}$ or GRAB$_{NE}$). For investigating the neuromodulator release in response to optogenetic activation of terminals, Chrimson was injected with a Hamilton beveled syringe (Reno, NV) into the LC (AP: -5.45, ML: -1.10, DV: -4.3 to -3.9) of the same mice as those which we were detecting behavioral neural dynamics. After injections, fiber optic ferrules (Doric) were chronically implanted above either the BLA or dCA1, and dental cement (Lang Dental, Wheeling, IL) or C&B Metabond was used to secure the implants. BLA and dCA1 implants and injections were done in the same mice. Mice were allowed to recover and viruses to express for a minimum of 5 weeks.

For investigating the neuromodulator release in response to optogenetic activation of terminals, the red-shifted channelrhodopsin ChrimsonR was injected with a Hamilton beveled syringe (Reno, NV) into the LC (AP: -5.45, ML: -1.10, DV: -4.3 to -3.9) of Th-cre mice (Th-cre::LC:Chrimson). To inhibit the VTA, the chemogenetic inhibitor AAV5-hSyn-DIO-HA-hM4D(Gi) was injected bilaterally in the VTA of the same Th-cre mice (Th-cre::VTA^{bilat}:Gi-DREADDs). For detecting NE and DA dynamics in the same Th-cre mice, 500nL of AAV1-hSyn-GRAB$_{NE2m}$-eGFP or AAV2/9-hSyn-WPRE-PA-GRAB$_{DA3m}$-eGFP were injected into dorsal CA1 (AP: 1.9, ML: -1.4, DV: -1.65) and the BLA (AP: -1.4, ML: -3.15, DV: -4.8 to -4.55) (Th-cre::BLA or CA1:GRAB$_{DA}$ or GRAB$_{NE}$). After injections, fiber optic ferrules (Doric) were chronically implanted above the dCA1 (AP: 1.9, ML: -1.4, DV: -1.65) and the BLA (AP: -1.4, ML: -3.15, DV: -4.8 to -4.55), and C&B Metabond was used to secure the implants. We waited five weeks for viruses to express before initiation of stimulation experiments.

For dual-color neuromodulator recordings, 500nL of AAV9-hSyn-GRAB$_{rDA2m}$ and AAV1-hSyn-GRAB$_{NE2m}$-eGFP were injected into dorsal CA1 (AP: 1.9, ML: -1.4, DV: -1.65) and the BLA (AP: -1.4, ML: -3.15, DV: -4.8 to -4.55) (Th-cre::BLA or CA1:GRAB$_{rDA}$ and GRAB$_{NE}$). We injected the cre-dependent chemogenetic inhibitor AAV5-hSyn1-DIO-HA-hM4D(Gi) bilaterally in the LC or VTA of Th-cre mice (Th-cre::LC^{bilat}:Gi-DREADDs) or (Th-cre::VTA^{bilat}:Gi-DREADDs). After injections, fiber optic ferrules (Doric) were chronically implanted above the dCA1 (AP: 1.9, ML: -1.4, DV: -1.65), and C&B Metabond was used to secure the implants. We waited five weeks for viruses to express before initiation of stimulation experiments.

Tissue collection and immunohistochemistry

After the conclusion of behavioral testing, mice were anesthetized with sodium pentobarbital and transcardially perfused with ice-cold PBS, followed by 4% phosphate-buffered paraformaldehyde. Brains were removed, postfixed overnight in 4% paraformaldehyde, and then saturated in 30% phosphate-buffered sucrose for 2–4 days at 4°C. Brains were sectioned at 30mM on a microtome and stored in a 0.01M phosphate buffer at 4°C prior to immunohistochemistry and tracing experiments. For behavioral cohorts, viral expression and optical fiber placements were confirmed before inclusion in the presented datasets. Viral expression and implant placements were verified using fluorescence and confocal (Leica Microsystems) microscopy. Images were produced with 10X, 20X, and 63X objectives and analyzed using ImageJ software (NIH) and Leica Application Suite Advanced Fluorescence software.

Looming stimulus

Adult mice were put in a custom-made open clear acrylic box, (50cm x 50cm) within a sound-attenuated room maintained at 23°C. The open box had white paper on all walls to limit outside stimuli. Mice were allowed to roam the box for 11 minutes prior to stimulus presentation to habituate to the box. At 11 minutes and in 60s intervals, a looming posterboard blocking overhead lighting was held over the arena for 10s. This was repeated 5 times. Fiber photometry was recorded for multiple biosensors detecting neural dynamics.

Reward retrieval and consumption

Mice were initially food deprived to 90% of their body weight. Prior to testing, we put multiple sucrose pellets per mouse in their home cage

to extinguish neophobia of this reward. On testing days, we placed mice in a modular (17.8×15.2×18.4cm^3; Med Associates Inc.) arena where they were allowed to freely roam. Using MEDPC program, we randomly delivered rewards at a pseudorandom ITI of 90-150s, with a total of 18 possible rewards in each session. Fiber photometry was recorded for multiple biosensors detecting neural dynamics.

Shock stimulus

Mice were placed in a modular arena and allowed to freely roam. After a baseline period of 180s in the arena, mice experienced the shock of a 0.5-0.7mA current run through the metal grating floor of the arena for 2s. There was a pseudorandom ITI of 20-90s, with 10 total shocks. Fiber photometry was recorded for multiple biosensors detecting neural dynamics. Video was recorded for the duration of the shock protocol and for 180s after. EzTrack(Pennington et al., 2019) was used to track and align freezing bouts for behavioral analysis.

In vivo fiber photometry

An optic fiber was secured to implanted fibers on experimental mice with a ferrule sleeve (Doric, ZR 2.5). Two light-emitting diodes (LEDs) were driven by a real-time processor (TDT, either RZ5P or RZ10x) that recorded dynamics from optic fibers detecting biosensor activity expressed in the brain, with 531-Hz sinusoidal 470nm (465nm on the RZ5P) and 211-Hz sinusoidal 405nm light. The 470nm LED was used to record emitted light from green sensors ($GRAB_{NE}$, dLight, and $GRAB_{DA}$) while the 405nm LED served as an isosbestic control. In dual sensor recordings taken with the RZ10x, 311-Hz sinusoidal 535nm light was used to record red sensors ($GRAB_{rDA}$). LED power for each LED wavelength were measured at the tip and adjusted to 30uW before each day of recording. For optogenetic stimulation, a 625nm LED was pulsed with 5ms pulse width for 3 or 30s. Laser power was adjusted to obtain 15mW transmittance into the brain.

Photometry analysis

A custom MATLAB script was developed for analysis of photometry recordings in the context of mouse behavior. For each photometry recording, a linear-least squares regression was used to find the projection of the isosbestic curve onto the 470 nm excitation photometry trace. The best fit isosbestic 405 nm excitation control signal was subtracted from the 470nm excitation signal to remove artifacts from intracellular NE-dependent sensor fluorescence(Lerner et al., 2015). Baseline drift was evident in the signal due to slow photobleaching artifacts, particularly the first several minutes of each recording session, and the linear least squares subtraction of the isosbestic control signal eliminated the drift seen in the 470nm excitation signal. After centering the signal around the first three minutes of the session, the photometry trace was z-scored relative to the mean and standard deviation of the test session. The post-processed fiber photometry signal was analyzed by time-locking each onset of behavior or stimulus, centering the data, and averaging the signal.

Ex vivo slice preparation

Mice were briefly anesthetized with isofluorane. Mice were perfused with cold N-methyl-d-glucamine (NMDG)–substituted artificial cerebrospinal fluid (aCSF) containing 93mM NMDG, 2.5mM KCl, 1.25mM NaH2PO4, 30mM NaHCO3, 20mM Hepes, 25mM glucose, 5mM ascorbic acid, 2mM thiourea, 3mM Na-pyruvate, 12mM N-acetyl-l-cysteine, 10mM MgSO4, and 0.5mM CaCl2. After perfusion, brains were extracted. Coronal sections of the hippocampus were cut to a slice thickness of 250µm using a vibrating Leica VT1000S microtome in a bath of cold, oxygenated NMDG solution. The slices were then placed in hot NMDG aCSF solution (32-34 degrees C) for 10min. Then slices were placed in a room temperature holding chamber filled with HEPES solution consisting of: 92mM NaCl, 2.5mM KCl, 1.2mM NaH2PO4, 30mM NaHCO3, 20mM Hepes, 25mM glucose, 2mM CaCl2, 2mM MgCl2 (pH adjusted to 7.3 to 7.4 with NaOH). The samples were kept in the HEPES solution for at least 30min prior to 2-photon imaging and were covered to minimize photobleaching. For both HEPES and NMDG osmolality was confirmed to be between 300-310mOsm/kg, and pH was confirmed to be between 7.3-7.4.

2-photon slice imaging, optogenetic stimulation, and pharmacology

Flow rate of ACSF or drug was maintained at 2mL/min. Temperature of flowing ACSF was controlled at 31-34 degrees C by the temperature controller TC-324C before any slice was added to the bath. An anchor was used to keep the brain slice stable while ACSF or ACSF and drug was washed on. A vacuum pump ensured a steady 2mL/s of flow. An Olympus 4x UPlanFL N lens was used to localize expression, and then an Olympus 20x XLPLN25XWMP lens 2mm working distance for water immersion, and we acquired images with Olympus FV31S-SW software. The 2-photon scope used was an FVMPE-RS Olympus 2p scope powered by a Mai Tai Ti-sapphire laser with dispersion compensation running at 920nm. Individual frames were acquired at 0.92hz using a Galvano scanner with a resolution of 512px x 512px. After setting up a slice on the 2-photon rig, we ran a positive control trial by washing high concentration (100µM) reactive ligand over the sensor-expressing slice. Once reactivity to the reactive ligand was confirmed, we allowed oxygenated ACSF to flow for 5 minutes for ligand to unbind from sensor. We next initiated optogenetic stimulation of brain slices using a 615nm red LED (CoolLED) controlled by a master-9 stimulator, programmed for either 5hz or 20hz stimulation for 3s or 30s, with a pulse-width of 5ms and limited to power of 3mW. Ligand solutions were oxygenated for at least 5min prior to washing on slices. Ligands were prepared with concentrations of between 3nM to 100µM.

Following optogenetic stimulation trials, we allowed oxygenated ACSF to flow over slices for at least 5 minutes for ligand to unbind from sensors before initiating ligand washes for concentration response curves. In some washes, we pumped ligand for 60s and recorded for two additional minutes to capture sensor binding and unbinding. We waited one minute between sessions of low concentration and 3-5min for higher concentration washes. We confirmed fluorescence resembled baseline of the previous session before initiating another wash,

and would alternate between high concentration ligand washes and low concentration washes (30µM, 10nM, 10µM, etc).

Pupillometry

Mice were anesthetized with 2% isofluorane. An infrared light was set up to record the mouse's pupil from a FLIR camera (1:1.4CCTV Lens, 9-22 mm lens with 1/3" focal length). Pupil contrast was carefully checked before recording session started. After 10min of recording for a baseline, we injected mice with either CNO (0.5 mg/kg i.p.) or saline vehicle. At least 45min after injection were recorded to track any changes in radii due to inhibition of the LC. We used a pupillometry analysis toolbox developed and described in Privitera et al., 2020.

DBH-KO mice experiments

A total of 40 Dbh(-/-)mice, maintained on a mixed 129/SvEv and C57BL/6 J background as previously described(Thomas et al., 1995; Thomas and Palmiter, 1997), were used in this study. *Dbh*(-/-) males were bred to *Dbh*(+/-) females, and pregnant *Dbh*(+/-) dams were administered drinking water containing the β-adrenergic receptor (AR) agonist isoproterenol and the α1AR agonist phenylephrine (20 µg/ml each; Sigma-Aldrich) with vitamin C (2 mg/ml) from E9.5E14.5, and the synthetic NE precursor L-3,4-dihydroxyphenylserine (DOPS; 2 mg/ml; Lundbeck, Deerfield, IL) + vitamin C (2 mg/ml) from E14.5-parturition to prevent embryonic lethality resulting from complete *Dbh* deficiency. *Dbh*(-/-) mice are easily distinguished from their NE-competent littermates by their visible delayed growth and bilateral ptosis phenotypes. *Dbh*(+/−) littermates were used as controls because their behavior and catecholamine levels 5 are indistinguishable from wild-type *Dbh*(+/+) mice(Bourdélat-Parks et al., 2005; Szot et al., 1999; Thomas and Palmiter, 1997). *Dbh*(-/-) males were bred to *Th*-cre females to produce *Th*-cre *Dbh*(-/-) mice. All animal procedures and protocols were approved by the Emory University Animal Care and Use Committee, in accordance with the National Institutes of Health guidelines for the care and use of laboratory animals. Mice were maintained on a 12 h/12 h light/dark cycle (7:00/19:00 h) with access to food and water ad libitum, except during behavioral testing. Behavioral testing was conducted under standard lighting conditions during the light cycle (14:00-17:00) in the same room where the mice were housed to minimize the stress of cage transport on test days. To record NE or DA dynamics, 500nL of AAV1-hSyn-GRAB$_{NE2m}$ (prepared in the UW NAPE center Viral Core, Seattle, WA) or AAV2/9-hSyn-GRAB$_{DA3m}$-WPRE-PA (Brain VTA) were injected with a Hamilton blunt syringe (Reno, NV) into CA1 (AP: 1.9, ML: -1.4, DV: -1.65) of *Dbh*(+/+)-cre, *Th*-cre *Dbh*(+/-), and *Th*-cre *Dbh*(-/-) mice. For inhibition experiments, AAV5-hSyn1-DIO-HA-hM4D (Gi) were injected bilaterally in the LC (AP: -5.45, ML: -1.10, DV: -4.3 to -3.9) or the VTA (15 degree angle, AP: -3.25, ML: -1.6, DV: -4.7 to -4.2). We waited five weeks for viruses to express before initiation of aversive and appetitive experiments. For investigating the neuromodulator release in response to optogenetic activation of terminals, the red-shifted channelrhodopsin ChrimsonR was injected with a Hamilton beveled syringe (Reno, NV) into the LC (AP: -5.45, ML: -1.10, DV: -4.3 to -3.9). After injections, fiber optic ferrules (Doric) were chronically implanted above the dCA1 (AP: 1.9, ML: -1.4, DV: -1.65), and C&B Metabond was used to secure the implants. We waited five weeks for viruses to express before initiation of stimulation experiments, done in accordance with photometry methods.

Quantification and statistical analysis

All data are expressed as mean ± SEM. Behavioral data were analyzed with GraphPad Prism 10.0 (GraphPad, La Jolla, CA). Two-tailed student's t test, one-way or two-way ANOVAs were used to analyze between-subjects designs. Repeated-measures designs were analyzed using a mixed-effects restricted maximum likelihood (REML) model. Tukey was used for post-hoc pairwise comparisons. The null hypothesis was rejected at the $p < 0.05$ level. Statistical significance was taken as $^{*}p < 0.05$, $^{**}p < 0.01$, $^{***}p < 0.005$, n.s. represents not significant. All statistical information is listed in Supplementary Table 1.

Acknowledgements

We thank Dr. Azra Suko for lab management and organization and Carina Pizzano, Akshay Rana, Bailey Wells, and Valerie Lau for assistance with the mouse colony. We thank Dr. Paul Phillips for feedback on sensor and genetic knockout experiments. We also thank the entire Bruchas laboratory as well as the Neuroscience of Addiction, Pain, and Emotion (NAPE) Center at the University of Washington for resources alongside critical feedback.

FUNDING

This work was supported by the National Institute of Mental Health (M.R.B., R01MH112355), the National Institute on Drug Abuse (A.K.M., F31DA056148; S.C.P., K99DA062328; I.R.R., E.G.S., P30DA048736), as well as the Mary Gates Research Scholarship (EGS). We thank UW NAPE center Viral Vector Core (P30-DA048736) and Azra Suko for virus preparation.

SUPPORTING INFORMATION

Additional supporting information may be found in the online version of the article.

SUPPLEMENTAL FIGURES

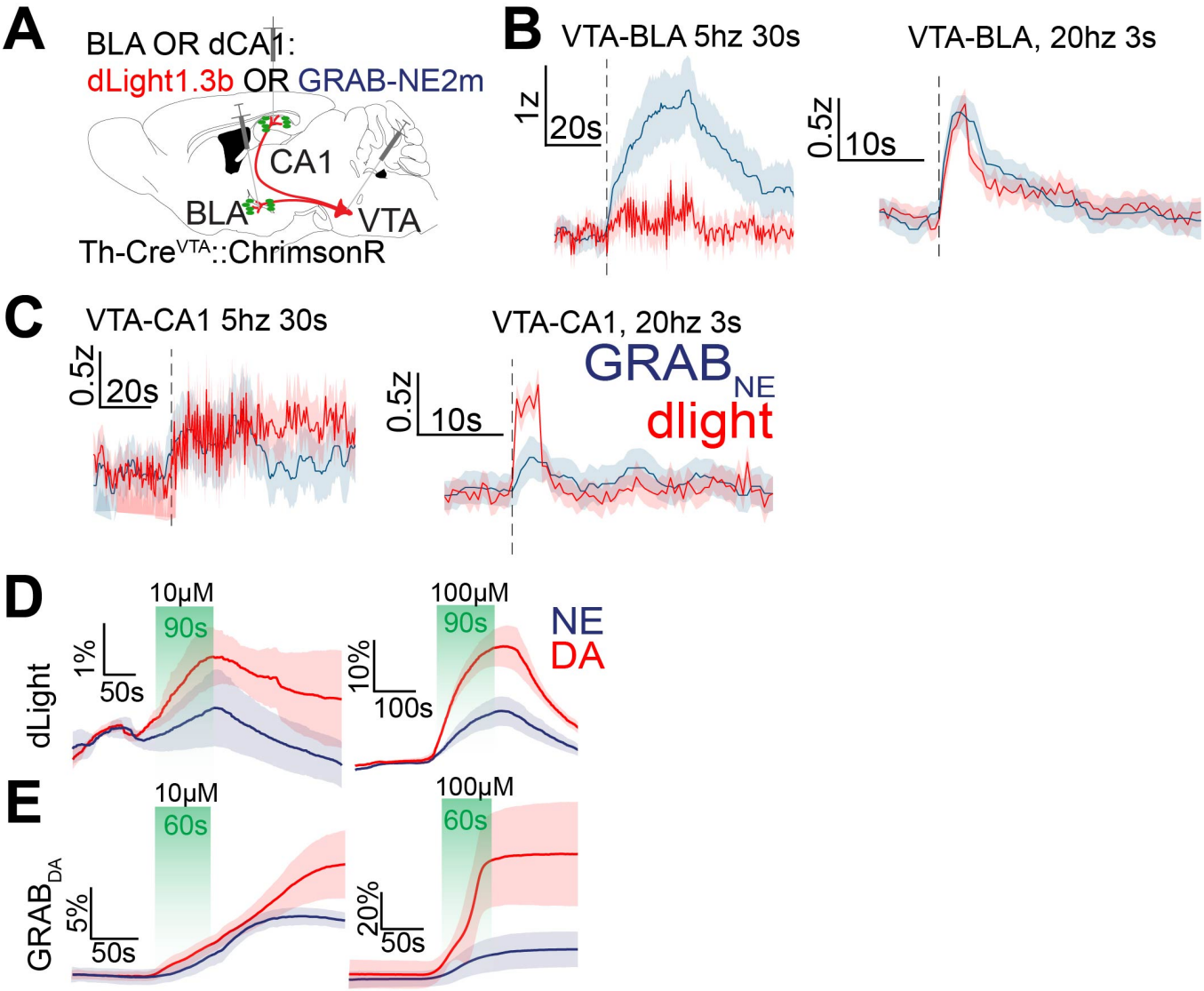

Supplemental Data Figure 1: Controls for biosensor selectivity

(a) Schematic of experimental approach of surgical injections for VTA terminal stimulation and recording photometric signals. Schematic depicts infection of VTA-DA cells with ChrimsonR (AAV5-hSyn-FLEX-ChrimsonR-tdTomato) and GRABNE or dLight in BLA (b) or CA1 (c). (b-c) Stimulation of VTA terminals in BLA (b) and CA1 (c), at 5hz for 30s (left) or 20hz for 3s (right). D-E. ΔF/F% change during DA and NE washes on dlight (G) or GRABDA (H) expressing slices at either 10μM (left) or 100μM (right).

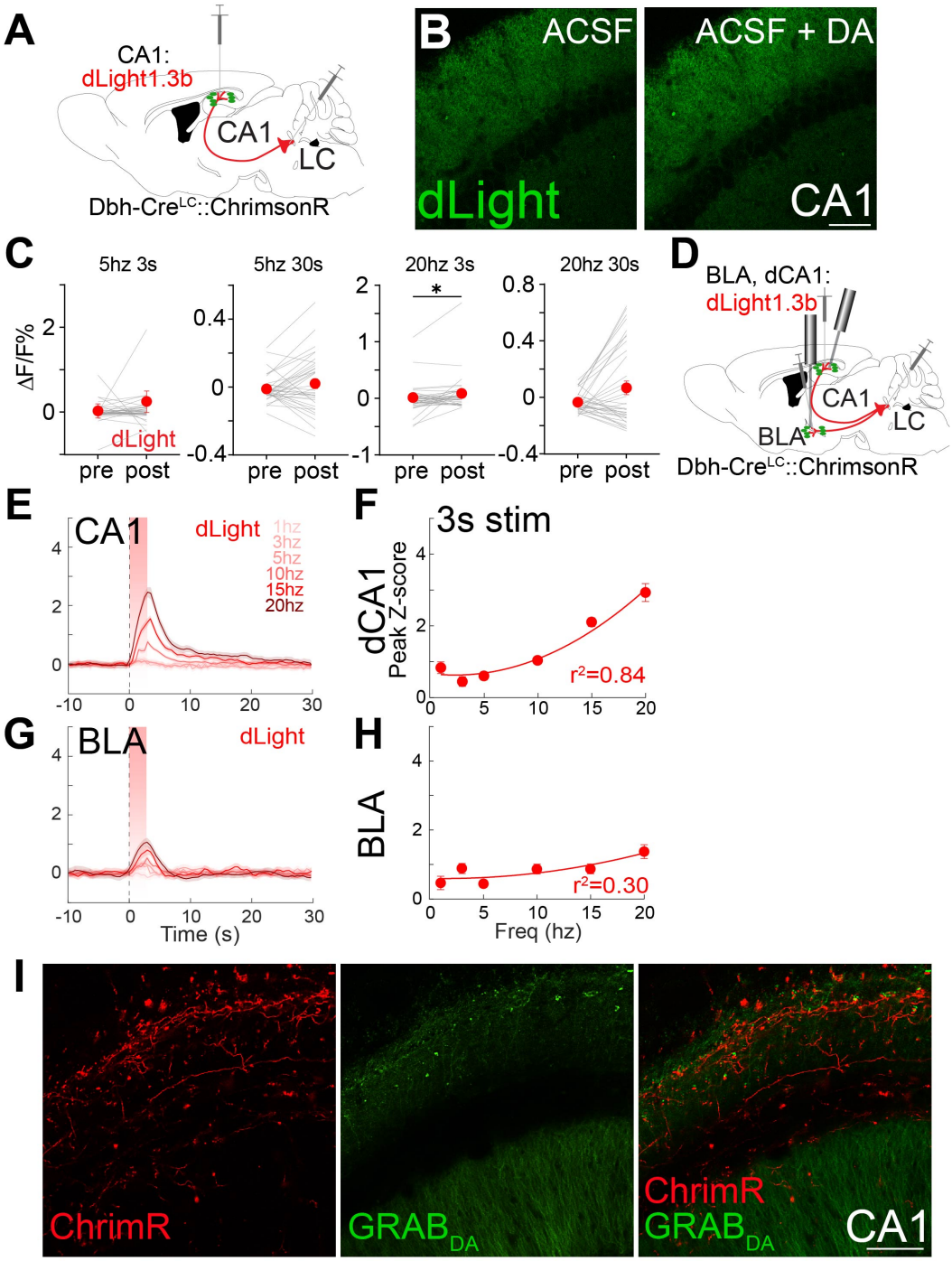

Supplemental Data Figure 2: LC-evoked DA is detected by dLight *in vivo* and *ex vivo*.

(a) Schematic of surgeries for 2-photon experiments with dLight. Chrimson was expressed in LC, and dLight in CA1. (b) Vehicle (left) and 30µM DA (right) washes on dLight expressing slices. Scale bar, 100µm. (c) ΔF/F% change from before to after stim in dlight (n=4 biological replicates, 6 slices) in response to a range of stimulation paradigms: 5hz 3s, 5hz 30s, 20hz 3s, 20hz 30s (left to right). Wilcoxon test, p=0.027. (d) Surgery schematic for in vivo optogenetic stimulation, with dLight expressed in CA1 and BLA and Chrimson expressed in LC. (e) dLight response to LC-CA1 stimulation at a range of frequencies (1-20hz). (f) Frequency response curves of dLight response when stimulating LC-CA1 terminals for 3s. Second-order curve fit to dLight, n=5-7, r^2= 0.84. (g) dLight response to LC-BLA stimulation at a range of frequencies (1-20hz). (h) Frequency response curves of dLight response when stimulating LC-BLA terminals for 3s. (i) Representative 2-photon image of virus expression in a hippocampal slice expressing GRABDA in CA1 and ChrimsonR in LC terminals in CA1. Scale bar, 100µm.

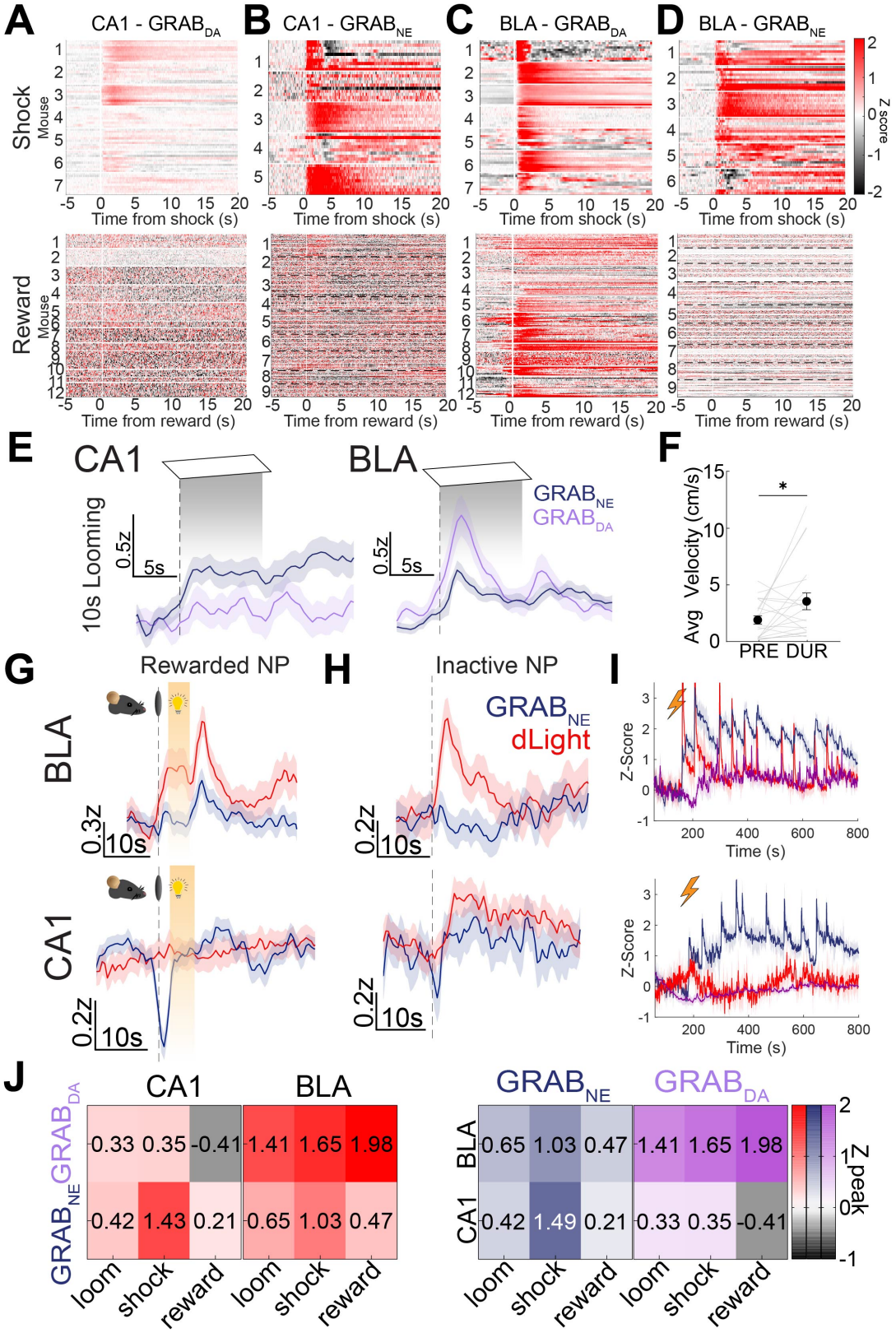

Supplemental Data Figure 3: NE and DA dynamics during aversive and appetitive behaviors

(a-d) Heatmaps of GRABDA and GRABNE response to shock (top) and reward (bottom) in BLA (a: GRABDA in CA1, b: GRABNE in CA1). (c-d) Heatmaps of GRABDA and GRABNE response to shock (top) and reward (bottom) in BLA (c: GRABDA in BLA, d: GRABNE in BLA). (e) NE (blue) and DA (purple) response to looming in CA1 (left) and BLA (right). (f) Mice dart at the first three looming stimuli presentations. Paired t-test, p=0.0364. (g-h) Response to nosepoking in the rewarded noseport (g), the unrewarded noseport (h) for BLA (top) or CA1 (bottom). (i) Full session recording of GRABDA (purple), GRABNE (blue), or dLight (red) during shock in BLA (top) or CA1 (bottom). (j) Heatmap of peak z-score in response to looming stimuli, shock, reward in CA1 and BLA.

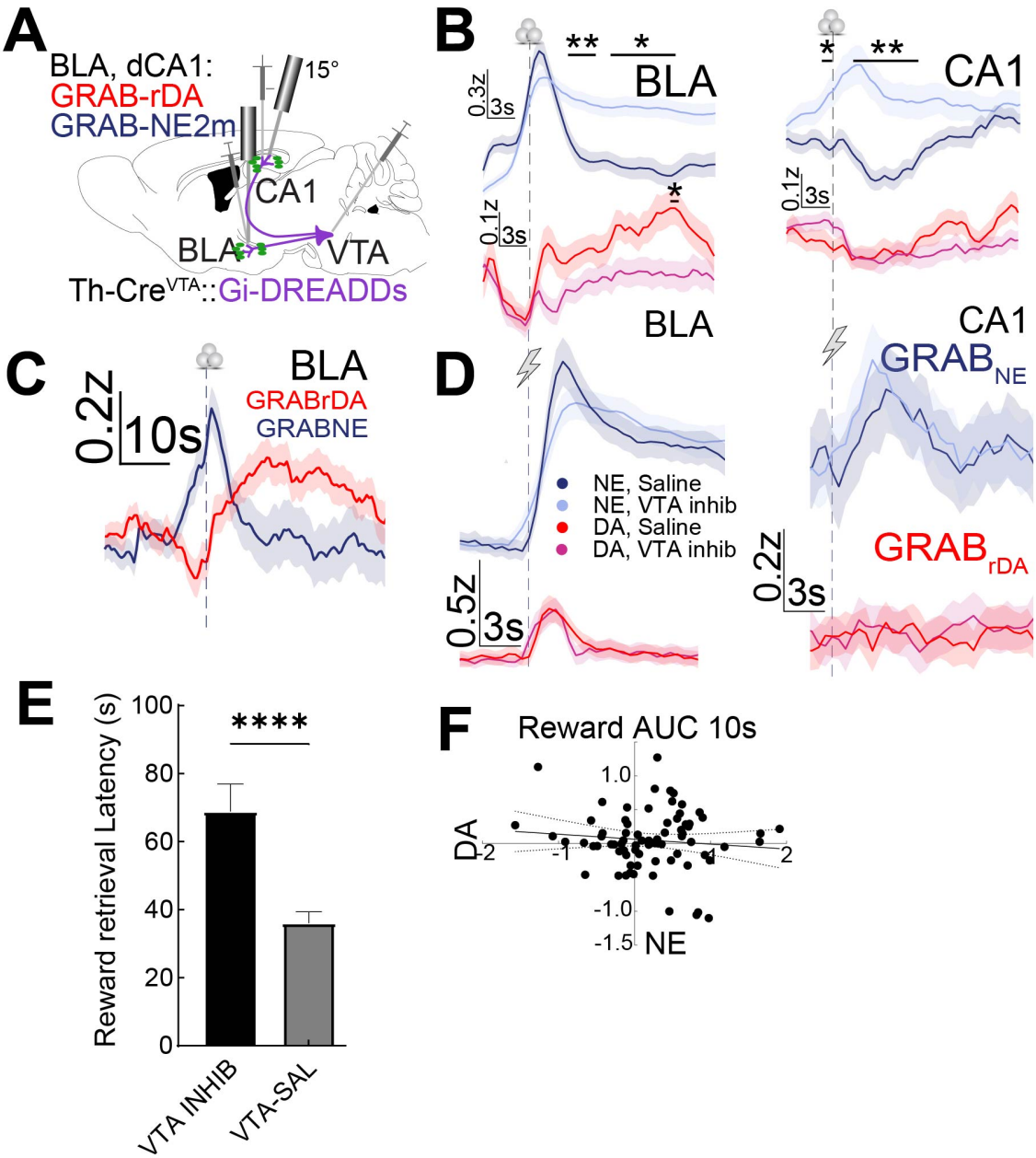

Supplemental Data Figure 4: VTA or LC inhibition effects on DA release in reward and shock.

(a) Schematic of surgeries preparing for recording DA and NE dynamics while inhibiting VTA. (b) DA response to reward in BLA (left) or CA1 (right) under VTA inhibition (magenta) or vehicle (red). (c) Latency to retrieve rewards following either saline or CNO administration, in mice expressing hM4Di in VTA. (d) Averaged, simultaneously recorded $GRAB_{rDA}$ and $GRAB_{NE}$ dynamics in BLA during reward retrieval prior to any neuromodulation. (e) AUC for 10s of DA vs AUC for 10s of NE after reward retrieval in Fig S4D. R^2=0.01. (f) DA response to shock in BLA (left) or CA1 (right) under VTA inhibition (magenta) or vehicle (red). Significance of 1s bins for all traces calculated using 2-way ANOVA with Sidak test for multiple comparisons, $p<0.05$.